Saudi Pharmaceutical Journal 31 (2023) 101803

HOSTED BY

Contents lists available at ScienceDirect

Saudi Pharmaceutical Journal

journal homepage: www.sciencedirect.com

Original article

Synthesis of novel spirochromane incorporating Schiff's bases, potential antiproliferative activity, and dual EGFR/HER2 inhibition: Cell cycle analysis and *in silico* study

Dina I.A. Othman [a], Abdelrahman Hamdi [a], Walaa M. Elhusseiny [a], Adel S. El-Azab [b], Ahmed H. Bakheit [b], Mohamed Hefnawy [b], Alaa A.-M. Abdel-Aziz [b,*]

[a] Department of Pharmaceutical Organic Chemistry, Faculty of Pharmacy, Mansoura University, Mansoura 35516, Egypt
[b] Department of Pharmaceutical Chemistry, College of Pharmacy, P.O. Box 2457, King Saud University, Riyadh 11451, Saudi Arabia

ARTICLE INFO

Article history:
Received 8 September 2023
Accepted 25 September 2023
Available online 28 September 2023

Keywords:
Spirochromane
Schiff's bases
Synthesis
Antiproliferative activity
Enzymatic assay
Apoptosis
Molecular docking

ABSTRACT

Spirochromanes incorporating Schiff's bases and semicarbazones **4a-e** and **5a-j** were synthesizedand analyzed for their potential antiproliferative activity using four human cancer cell lines (MCF-7, HCT-116, PC3, and A549). Compounds **5a**, **5b** and **5g** possessed the highest antiproliferative activity among the tested compounds,with an IC_{50} range of 1.154–9.09 μM. Compound **5j** selectively inhibited the PC3 cell proliferation (IC_{50} = 5.47 μM). Spirochromanes **5a**, **5b** and **5g** exhibited high inhibitory activity against EGFR (IC_{50} = 0.116, 0.132, and 0.077 μM, respectively) and HER2 (IC_{50} = 0.055, 0.210 and 0.085 μM, respectively) compared with the references, erlotinib (IC_{50} = 0.090 and 0.038 μM, respectively) and gefitinib (IC_{50} = 0.052 and 0.072 μM, respectively). Cell cycle analysis and apoptosis results showed that compounds **5a**, **5b** and **5g** arrested growth inthe S phase, and the programmed cell death induced by these compounds was an apoptotic mechanism rather than a necrotic pathway. Molecular docking studies of spirochromanes **5a**, **5b** and **5g** to EGFR and HER2 binding sites were performed to explore the orientation mode and interaction.

1. Introduction

Cancer is one of the leading public health problems worldwide, and many people are diagnosed with cancer annually (Torre et al., 2015; El-Husseiny et al., 2018; El-Azab et al., 2017; Al-Suwaidan et al., 2016; Hamdi et al., 2016). The use of chemotherapy in cancer treatment has become the traditional treatment; however, many cases exhibit no efficacy owing to poor selectivity and drug resistance, resulting in severe side effects (Holohan et al., 2013; Housman et al., 2014). Consequently, novel and effective anticancer agents are urgently required (El-Sherbeny et al., 2010; Alanazi et al., 2013; El-Azab et al., 2013; Mohammed et al., 2016). Moreover, the use of drug combinations in cancer treatment has several undesirable effects (Szakács et al., 2006; Bayat Mokhtari et al., 2017), which can be overcome by the preferred therapeutic strategy that involves using a single compound with multiple molecular mechanisms (Alkahtani et al., 2020; El-Azab et al., 2018; Fu et al., 2017; Antonello et al., 2006). Therefore, a single compound with multiple molecular mechanisms is used in a current trend therapy as multitargeted therapy (Xie and Bourne, 2015). In cell signalling pathways, survival of the cancer cell is enhanced through the activation of many kinases such as EGFR (epidermal growth factor receptor) and HER2 (human epidermal growth factor receptor 2) (Baker and Reddy, 2010; Christensen et al., 2007; Black, et al., 2003; Abdelsalam et al., 2019). Targeting these kinases is a must to produce potent and efficient anticancer agents (Regad, 2015; Woodburn, 1999; Rusnak, et al., 2001; El-Azab, et al., 2020). In addition, apoptosis was found in various solid tumors due to the inhibition of the tyrosine kinases (Alkahtani et al., 2020; Gullick, 1991).

Sorafenib (Nexavar®), Gefitinib (Iressa®), Erlotinib (Tarceva®), Lapatinib (Tykerb®) and Vandetanib (Caprelsa®) are multikinase inhibitors that have been approved as chemotherapeutic agents with high selectivity and efficacy (Fig. 1) (Wang et al., 2017; Omar et al., 2016; Gundla, et al., 2008; Madhusudan and Ganesan, 2004; Barker et al., 2001; Frampton et al., 2009;

* Corresponding author.
E-mail address: almoenes@ksu.edu.sa (A.A.-M. Abdel-Aziz).
Peer review under responsibility of King Saud University.

ELSEVIER Production and hosting by Elsevier

https://doi.org/10.1016/j.jsps.2023.101803
1319-0164/

Takimoto and Awada, 2008; Dungo and Keating, 2013). On the other hand, spirochromanes and spirochromane piperidines **I**, **II** and **III** (Fig. 2) possess potent anticancer activity (Uto et al., 2010; Varasi et al., 2011). Also, compounds incorporating an aldimine or ketimine moiety (RHC = N-R) (Fig. 2), such as Schiff's bases, hydrazones and semicarbazones, have been characterized as efficient anticancer agents (compounds **IV**, V, and VI) (Xu et al., 2008; Abdel-Aziz et al., 2021;Krishnan et al., 2008; Peterson, et al., 2009). Some of these compounds inhibit EGFR and HER2 and induce apoptosis (Şenkardeş et al., 2020; Vogel et al., 2008; George, 2018).

Based on the aforementioned rationale, novel spirochromane piperidine derivatives **4a-e** and **5a-j** incorporating Schiff's bases (Fig. 2) were synthesized, and their antiproliferative activities were evaluated using the 3-[4,5-dimethylthiazol-2-yl]-2,5-diphenyl tetrazolium bromide (MTT) assay. Structure-activity relationship (SAR) was also studied in diverse chemical spaces. In addition, the EGFR and HER2 inhibition assay for derivatives with promising antiproliferative activity was performed. Next, apoptosis and cell cycle status in tissue culture cell lines were determined by measuring the DNA content by flow cytometry. A docking protocol inside the binding sites of EGFR and HER2 tyrosine kinases was conducted to determine the binding modes of the promising compounds.

2. Material and methods

2.1. Chemistry

The melting points of the compounds (°C) were determined using a Stuart melting point apparatus (SMP 30). Infrared (IR) spectra were measured on an FT-IR 200 spectrophotometer (ύ cm^{-1}) Faculty of Pharmacy, Mansoura University. The ^{1}H NMR and ^{13}C NMR spectra were recorded in $CDCl_3$ or DMSO d_6 at $^{1}HNMR$ (400 MHz) and $^{13}CNMR$ (100 MHz) on a Bruker NMR spectrometer (δ ppm) using tetramethylsilane(TMS) as an internal standard at the NMR Unit, Faculty of Pharmacy, Mansoura University. Mass spectra were obtained using the direct inlet of a mass analyzer in a Thermo Scientific GC/MS model ISQ at the Regional Center for Mycology and Biotechnology (RCMB), Al-Azhar University, Egypt. The cell cycle analysis was performed using a confirmatory diagnostic unit (VACSERA, Egypt). Compounds **2a** and **b** were prepared as previously described (Battisti et al., 2014).

2.1.1. General procedure for preparation of hydrazone derivatives 3a,b

Hydrazine hydrate (3.6 mmol) in ethanol (20 ml) was added to a solution of spirochromanone derivatives **2a**,**b** (3 mmol), and the mixture was left to stir at room temperature for 5 h.The reaction mixture was concentrated using a Rotavap, water was added, extracted with ethyl acetate (10 ml × 3) and evaporated under reduced pressure to generate yellow solids, which were used directly for the next step without any further purification.

2.1.1.1. (E)-4-Hydrazono-1′-methylspiro[chroman-2,4′-piperidine] (3a). Yellow solid; (65%). M.p. 110 – 112 °C. IR (νmax/cm^{-1}): 3345, 3400 (NH_2), 3139, 2972, 2936 (CHs), 1615 (C = N), 1450, 1234, 1180. ^{1}H NMR (400 MHz, $CDCl_3$) δ 7.87 (dd, J = 7.9, 1.3 Hz, 1H), 7.24 – 7.19 (m, 1H), 6.97 – 6.89 (m, 2H), 5.31 (s, 2H), 2.60 (s, 2H), 2.53 (s, 2H), 2.40 (dd, J = 16.4, 6.7 Hz, 2H), 2.33 (s, 3H), 1.98 (d, J = 12.2 Hz, 2H), 1.70 (td, J = 13.7, 4.4 Hz, 2H). ^{13}C NMR

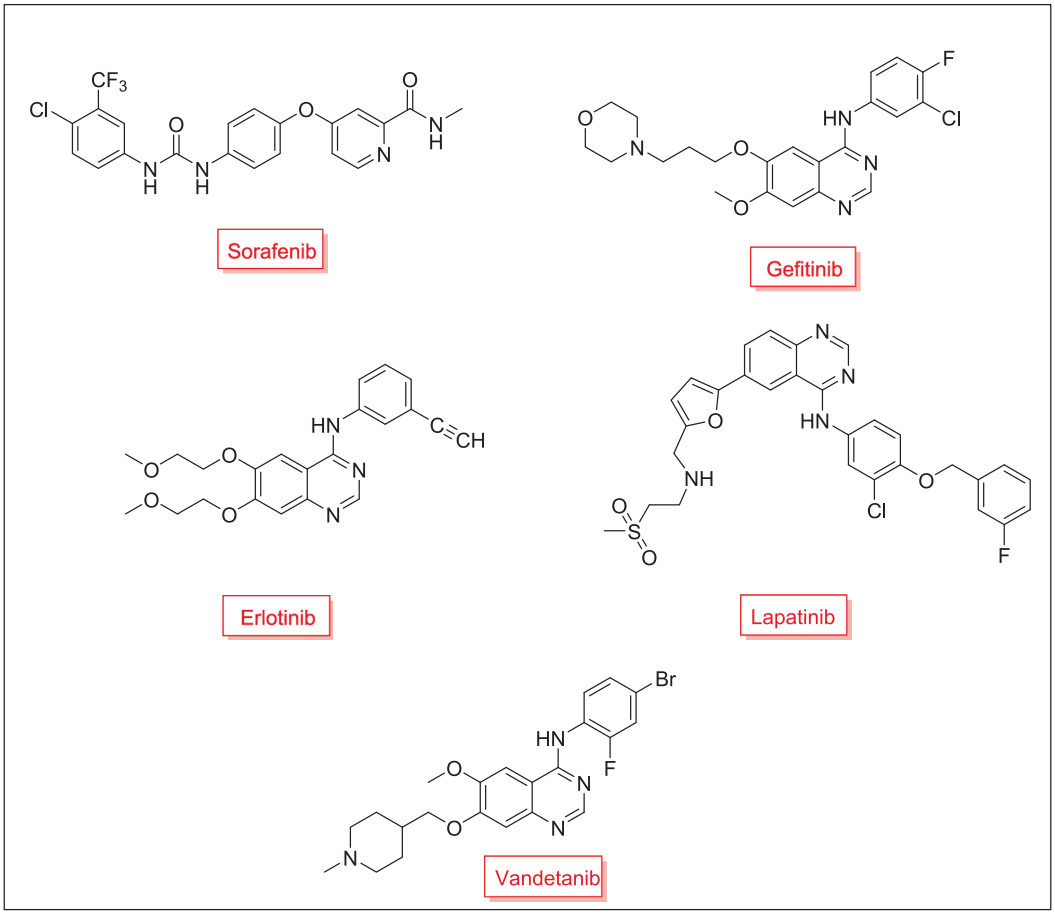

Fig. 1. Approved multikinase inhibitors as chemotherapeutic agents.

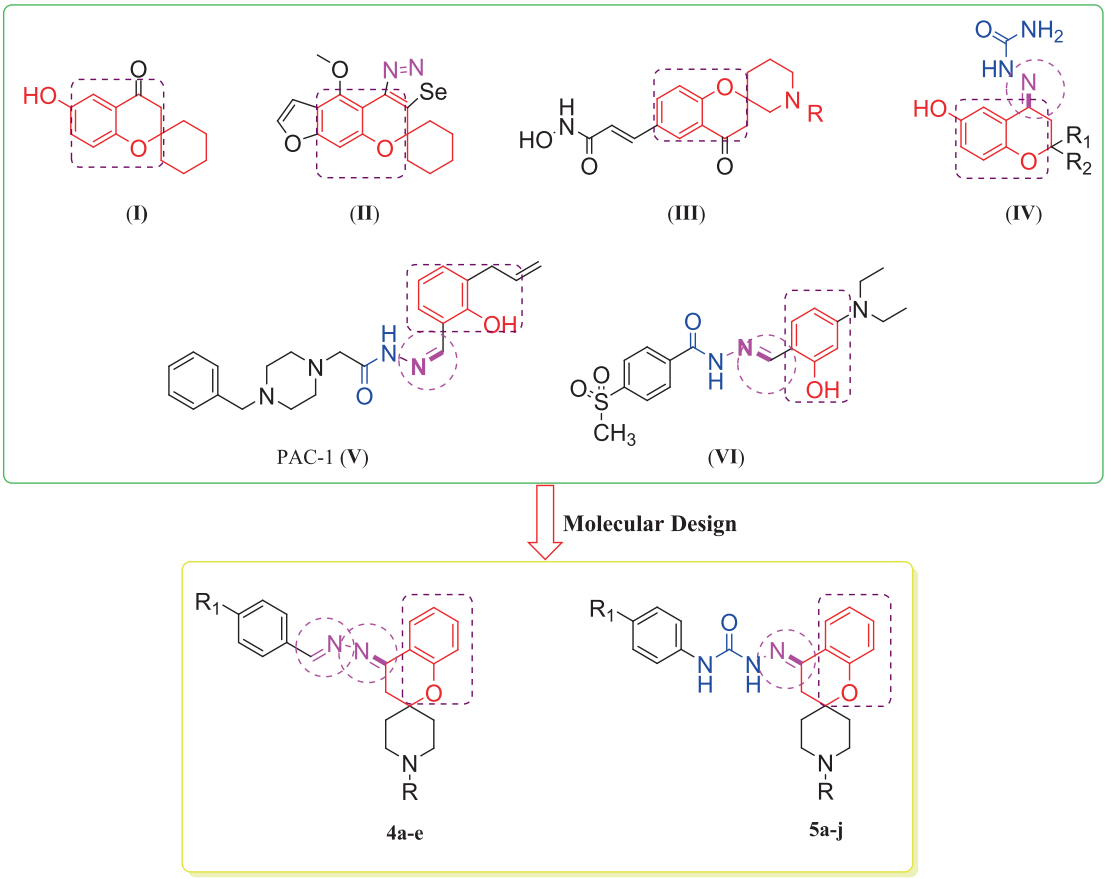

Fig. 2. Reported anticancer spirochromanes (**I-III**), Schiff's bases (**IV**, **V** and **VI**) and the designed compounds (**4a-e** and **5a-j**).

(100 MHz, $CDCl_3$) δ 152.8, 141.0, 132.2, 129.9, 123.7, 122.1, 118.0, 72.6, 50.9, 45.8, 34.4, 34.1. MS *m*/*z* (%): 245.15 (M^+, 17.88).

2.1.1.2. (E)-1′-Ethyl-4-hydrazonospiro[chroman-2,4′-piperidine] (3b). Brown solid; (55%). M.p. 100–102 °C. IR (νmax/cm^{-1}): 3338,3400 (NH_2), 3134, 2971, 2936 (CHs), 1609 (C = N), 1454, 1234, 1181. ^{1}H NMR (400 MHz, $CDCl_3$) δ 7.87 (dd, *J* = 7.9, 1.3 Hz, 1H), 7.25 – 7.19 (m, 1H), 6.98 – 6.89 (m, 2H), 5.31 (s, 2H), 2.69 (d, *J* = 11.5 Hz, 2H), 2.53 (s, 2H), 2.48 (q, *J* = 7.2 Hz, 2H), 2.43 – 2.37 (m, 2H), 1.99 (d, *J* = 12.3 Hz, 2H), 1.76 – 1.67 (m, 2H), 1.12 (t, *J* = 7.2 Hz, 3H). ^{13}C NMR (100 MHz, $CDCl_3$) δ 153.0, 140.8, 132.0, 129.9, 123.7, 122.1, 118.5, 72.3, 50.2, 48.8, 34.4, 34.1, 12.9. MS *m*/*z* (%): 259.32 (M^+, 26.03).

2.1.2. General procedure for preparation of hydrazone derivatives 4a-e

A mixture of hydrazone derivatives **3a**,**b** (1.0 mmol), appropriate aldehyde (1.0 mmol) and catalytic drops of glacial acetic acid in ethanol (20 ml) was heated under reflux overnight. The reaction mixture was allowed to cool and then poured into icewater (60 ml). The resulting precipitate was collected, washed with water and recrystallized from ethanol.

2.1.2.1. (E)-4-[(E)-(4-Chlorobenzylidene)hydrazono]-1′-methylspiro (chroman-2,4′-piperidine) (4a). White solid; (73%). M.p. 139–141 °C. IR (νmax/cm^{-1}): 3062, 2938 (CHs), 1616 (C=N), 1455, 1229, 1180. ^{1}H NMR (400 MHz, $CDCl_3$) δ 8.50 (s, 1H), 8.15 (d, *J* = 6.9 Hz, 1H), 7.79 (d, *J* = 8.4 Hz, 2H), 7.44 (d, *J* = 8.4 Hz, 2H), 7.37 (t, *J* = 7.1 Hz, 1H), 7.02 – 6.96 (m, 2H), 3.14 (s, 2H), 2.61 (d, *J* = 11.4 Hz, 2H), 2.44 (t, *J* = 10.7 Hz, 2H), 2.34 (s, 3H), 2.01 (d, *J* = 13.1 Hz, 2H), 1.80 (d, *J* = 4.5 Hz, 2H). ^{13}C NMR (100 MHz, DMSO d_6) δ 159.1, 158.1, 155.81 (s), 136.1, 133.7, 133.3, 130.4, 129.4, 125.1, 121.2, 120.0, 118.5, 74.9, 51.0, 46.3, 35.8, 34.3. MS *m*/*z* (%): 367.69 (M^+, 18.63).

2.1.2.2. 2.1.2.2.N,N-Dimethyl-4-((E)-{(E)-[1′-methylspiro(chroman-2,4′-piperidin)-4-ylidene]hydrazono}methyl)aniline (4b). White solid; (60%). M.p. 155–157 °C. IR (νmax/cm^{-1}): 3060, 2940 (CHs), 1618 (C=N), 1450, 1220, 1189. ^{1}H NMR (400 MHz, $CDCl_3$) δ 8.48 (s, 1H), 8.16 (d, *J* = 6.8 Hz, 1H), 7.73 (d, *J* = 7.7 Hz, 2H), 7.34 (t, *J* = 7.7 Hz, 1H), 7.03 – 6.93 (m, 2H), 6.75 (d, *J* = 7.7 Hz, 2H), 3.19 (s, 2H), 3.07 (s, 6H), 2.61 (d, *J* = 11.4 Hz, 2H), 2.44 (t, *J* = 10.5 Hz, 2H), 2.34 (s, 3H), 2.00 (d, *J* = 13.0 Hz, 2H), 1.81 (d, *J* = 4.2 Hz, 2H). ^{13}C NMR (100 MHz, $CDCl_3$) δ 160.1, 157.2, 155.2, 152.3, 132.0, 130.1, 125.0, 122.4, 120.9, 120.5, 118.0, 111.7, 74.0, 51.0, 45.9, 40.2, 36.1, 34.2.MS *m*/*z* (%): 376.99 (M^+, 19.99).

2.1.2.3. 4-((E)-{(E)-[1′-Ethylspiro(chroman-2,4′-piperidin)-4-ylidene] hydrazono}methyl)-N,N-dimethylaniline (4c). White solid; (58%). M.p. 110–112 °C. IR (νmax/cm^{-1}): 3058, 2945 (CHs), 1620 (C=N), 1450, 1225, 1110. ^{1}H NMR (400 MHz, $CDCl_3$) δ 8.48 (s, 1H), 8.18 (d, *J* = 7.7 Hz, 1H), 7.74 (d, *J* = 8.5 Hz, 2H), 7.38 – 7.32 (m, 1H), 7.00 (t, *J* = 7.3 Hz, 1H), 6.94 (d, *J* = 8.1 Hz, 1H), 6.75 (d, *J* = 8.5 Hz, 2H), 3.23 (s, 2H), 3.07 (s, 6H), 2.97 – 2.90 (m, 2H), 2.72 – 2.64 (m, 4H), 2.06 (s, 4H), 1.25 (t, *J* = 7.2 Hz, 3H). MS *m*/*z* (%): 390.45 (M^+, 26.70).

4-((E)-{(E)-[1′-Methylspiro(chroman-2,4′-piperidin)-4-ylidene] hydrazono}methyl)phenol (4d).

White solid; (52%). M.p. 166–168 °C. IR (νmax/cm^{-1}): 3538 (OH), 3064, 2947 (CHs), 1609 (C=N), 1513, 1457, 1160. ^{1}H NMR (400 MHz, $CDCl_3$) δ 8.48 (s, 1H), 8.16 (d, *J* = 7.4 Hz, 1H), 7.73 (d, *J* = 8.4 Hz, 2H), 7.36 (t, *J* = 7.2 Hz, 1H), 7.04 – 6.93 (m, 2H), 6.86 (d, *J* = 8.4 Hz, 2H), 3.15 (s, 2H), 3.00 (s, 1H), 2.77 (d, *J* = 11.1 Hz,

2H), 2.55 (t, *J* = 11.4 Hz, 2H), 2.42 (s, 3H), 2.03 (d, *J* = 13.3 Hz, 2H), 1.82 (t, *J* = 11.2 Hz, 2H). MS *m*/*z* (%): 349.34 (M^+, 25.21).

4-((E)-{(E)-[1′-Ethylspiro(chroman-2,4′-piperidin)-4-ylidene]hydrazon}methyl)phenol (4e).

White solid; (50%). M.p. 135–137 °C. 3540 (OH), 3064, 2940 (CHs), 1612 (C=N), 1513, 1457, 1180. ^{1}H NMR (400 MHz, $CDCl_3$) δ 8.46 (s, 1H), 8.19 – 8.12 (m, 1H), 7.71 (d, *J* = 8.4 Hz, 2H), 7.38 – 7.32 (m, 1H), 7.00 (t, *J* = 7.5 Hz, 1H), 6.94 (d, *J* = 8.2 Hz, 1H), 6.87 (d, *J* = 8.4 Hz, 2H), 5.02 (s, 1H), 3.15 (s, 2H), 2.92 (d, *J* = 11.3 Hz, 2H), 2.69 – 2.52 (m, 4H), 2.09 – 2.00 (m, 2H), 1.87 (dd, *J* = 19.4, 6.8 Hz, 2H), 1.21 (t, *J* = 7.2 Hz, 3H). ^{13}C NMR (100 MHz, $CDCl_3$) δ 160.4, 159.5, 157.9, 155.2, 132.3, 130.5, 126.1, 125.2, 121.1, 120.2, 117.9, 116.4, 74.2, 52.2, 48.1, 36.3, 33.4, 11.3.MS *m*/*z* (%): 363.80 (M^+, 15.63).

2.1.3. General procedure for preparation of hydrazone derivatives 5a-j

The appropriate phenyl isocyanate derivative (2.0 mmol) was added to a solution of the hydrazone derivatives **3a,b** (2.0 mmol) in THF (20 ml). The reaction mixture was stirred overnight at room temperature. After reaction completion was confirmed by thin layer chromatography, the reaction mixture was poured onto ice. The resulting solids were separated and recrystallized from ethanol.

2.1.3.1. (E)-2-(1′-Methylspirochroman-2,4′-piperidin-4-ylidene)-N-phenyl hydrazine carboxamide (5a). White solid; (73%). M.p. 233–235 °C. IR (νmax/cm^{-1}): 3368, 3203 (NHs), 3104, 2936 (CHs), 1679 (C=O), 1597, 1538, 1128. ^{1}H NMR (400 MHz, DMSO d_6) δ 9.93 (s, 1H), 8.95 (s, 1H), 8.28 (d, *J* = 6.9 Hz, 1H), 7.66 (d, *J* = 7.9 Hz, 2H), 7.35 – 7.26 (m, 3H), 7.04 (t, *J* = 7.4 Hz, 1H), 6.98 (t, *J* = 7.5 Hz, 1H), 6.90 (d, *J* = 8.2 Hz, 1H), 2.85 (s, 2H), 2.47 (d, *J* = 11.4 Hz, 2H), 2.32 (t, *J* = 9.5 Hz, 2H), 2.21 (s, 3H), 1.79 (d, *J* = 13.6 Hz, 2H), 1.64 (t, *J* = 9.7 Hz, 2H). ^{13}C NMR (100 MHz, DMSO d_6) δ 154.2, 154.0, 140.3, 139.5, 131.3, 128.9, 125.4, 123.1, 121.2, 120.6, 120.5, 118.2, 74.2, 50.9, 46.2, 34.6, 34.5.MS *m*/*z* (%): 364.25 (M^+, 20.73).

(E)-2-(1′-Ethylspirochroman-2,4′-piperidin-4-ylidene)-N-phenyl hydrazine carboxamide (5b).

White solid; (69%). M.p. 228–230 °C. IR (νmax/cm^{-1}): 3365, 3220 (NHs), 3110, 2930 (CHs), 1680 (C=O), 1597, 1538, 1120. ^{1}H NMR (400 MHz, DMSO d_6) δ 9.93 (s, 1H), 8.95 (s, 1H), 8.28 (d, *J* = 7.8 Hz, 1H), 7.66 (d, *J* = 7.9 Hz, 2H), 7.37 – 7.27 (m, 3H), 7.05 (t, *J* = 7.3 Hz, 1H), 6.98 (t, *J* = 7.5 Hz, 1H), 6.89 (d, *J* = 8.1 Hz, 1H), 2.85 (s, 2H), 2.56 (s, 2H), 2.37 (q, *J* = 7.1 Hz, 2H), 2.34 – 2.29 (m, 2H), 1.79 (d, *J* = 13.8 Hz, 2H), 1.63 (t, *J* = 9.9 Hz, 2H), 1.02 (t, *J* = 7.1 Hz, 3H). ^{13}C NMR (100 MHz, DMSO d_6) δ 154.3, 154.0, 140.4, 139.5, 131.3, 128.9, 125.3, 123.1, 121.2, 120.7, 120.5, 118.2, 74.8, 51.9, 48.5, 34.7, 34.6, 12.7.MS *m*/*z* (%): 378.60 (M^+, 13.65).

2.1.3.2. (E)-N-(4-Chlorophenyl)-2-(1′-methylspirochroman-2,4′-piperidin)-4-ylidene hydrazine carboxamide (5c). White solid; (78%). M.p. 250–252 °C. IR (νmax/cm^{-1}): 3368, 3205 (NHs), 3110, 2938 (CHs), 1678 (C=O), 1590, 1200, 1128. ^{1}H NMR (400 MHz, DMSO d_6) δ 10.01 (s, 1H), 9.09 (s, 1H), 8.30 (d, *J* = 7.0 Hz, 1H), 7.73 (d, *J* = 8.8 Hz, 2H), 7.37 (d, *J* = 8.8 Hz, 2H), 7.29 (t, *J* = 7.0 Hz, 1H), 6.98 (t, *J* = 7.4 Hz, 1H), 6.90 (d, *J* = 8.2 Hz, 1H), 2.85 (s, 2H), 2.47 (d, *J* = 11.6 Hz, 2H), 2.32 (t, *J* = 9.4 Hz, 2H), 2.21 (s, 3H), 1.81 – 1.74 (m, 2H), 1.64 (t, *J* = 9.7 Hz, 2H). ^{13}C NMR (100 MHz, DMSO d_6) δ 154.3, 154.0, 140.7, 138.6, 131.5, 128.8, 126.6, 125.5, 122.1, 121.2, 120.5, 118.2, 74.2, 50.9, 46.2, 34.5, 34.4.MS *m*/*z* (%): 398.82 (M^+, 25.63).

2.1.3.3. (E)-N-(4-Chlorophenyl)-2-(1′-ethylspirochroman-2,4′-piperidin-4-ylidene)hydrazine carboxamide (5d). White solid; (74%). M.p. 242–244 °C. IR (νmax/cm^{-1}): 3360, 3203 (NHs), 3104, 2940 (CHs), 1679 (C=O), 1597, 1530, 1128. ^{1}H NMR (400 MHz, DMSO d_6) δ 10.01 (s, 1H), 9.09 (s, 1H), 8.29 (d, *J* = 7.8 Hz, 1H), 7.73 (d, *J* = 8.7 Hz, 2H), 7.37 (d, *J* = 8.7 Hz, 2H), 7.29 (t, *J* = 7.5 Hz, 1H), 6.97 (t, *J* = 7.5 Hz, 1H), 6.89 (d, *J* = 8.0 Hz, 1H), 2.85 (s, 2H), 2.53 (s, 2H), 2.37 (q, *J* = 7.1 Hz, 2H), 2.34 – 2.29 (m, 2H), 1.78 (d, *J* = 12.9 Hz, 2H), 1.63 (t, *J* = 7.1 Hz, 2H), 1.01 (t, *J* = 7.1 Hz, 3H). ^{13}C NMR (101 MHz, DMSO d_6) δ 154.2, 153.9, 140.7, 138.6, 131.4, 128.8, 126.6, 125.6, 122.2, 121.1, 120.6, 118.2, 74.8, 52.0, 48.5, 34.6, 34.5, 12.8.MS *m*/*z* (%): 412.75 (M^+, 27.73).

2.1.3.4. (E)-2-(1′-Methylspirochroman-2,4′-piperidin-4-ylidene)-N-(4-nitrophenyl)hydrazine carboxamide (5e). White solid; (61%). M.p. 270–272 °C. IR (νmax/cm^{-1}): 3370, 3203 (NHs), 3109, 2930 (CHs), 1679 (C=O), 1597, 1500, 1128. ^{1}H NMR (400 MHz, DMSO d_6) δ 10.27 (s, 1H), 9.58 (s, 1H), 8.30 (d, *J* = 7.1 Hz, 1H), 8.24 (d, *J* = 9.2 Hz, 2H), 8.01 (d, *J* = 9.2 Hz, 2H), 7.37 – 7.27 (m, 1H), 7.00 (t, *J* = 7.5 Hz, 1H), 6.91 (d, *J* = 8.1 Hz, 1H), 2.87 (s, 2H), 2.47 (d, *J* = 11.3 Hz, 2H), 2.32 (t, *J* = 9.5 Hz, 2H), 2.21 (s, 3H), 1.79 (d, *J* = 14.4 Hz, 2H), 1.65 (t, *J* = 7.1 Hz, 2H). ^{13}C NMR (100 MHz, DMSO d_6) δ 154.4, 153.6, 146.2, 142.1, 141.7, 131.7, 125.6, 125.2, 121.2, 120.4, 119.6, 118.2, 74.2, 50.9, 46.2, 34.5, 29.5.MS *m*/*z* (%): 409.23 (M^+, 15.69).

2.1.3.5. (E)-2-(1′-Ethylspirochroman-2,4′-piperidin-4-ylidene)-N-(4-nitrophenyl)hydrazine carboxamide (5f). White solid; (63%). M.p. 247–249 °C. IR (νmax/cm^{-1}): 3346, 3201 (NHs), 3108, 2939 (CHs), 1693 (C=O), 1603, 1543, 1117. ^{1}H NMR (400 MHz, DMSO d_6) δ 10.26 (s, 1H), 9.58 (s, 1H), 8.30 (d, *J* = 7.8 Hz, 1H), 8.24 (d, *J* = 8.9 Hz, 2H), 8.01 (d, *J* = 8.9 Hz, 2H), 7.31 (t, *J* = 7.4 Hz, 1H), 7.00 (t, *J* = 7.4 Hz, 1H), 6.90 (d, *J* = 8.1 Hz, 1H), 2.87 (s, 2H), 2.53 (s, 2H), 2.37 (q, *J* = 7.1 Hz, 2H), 2.34 – 2.29 (m, 2H), 1.79 (d, *J* = 14.4 Hz, 2H), 1.63 (t, *J* = 9.7 Hz, 2H), 1.01 (t, *J* = 7.1 Hz, 3H). ^{13}C NMR (100 MHz, DMSO d_6) δ 154.4, 153.6, 146.2, 142.1, 141.7, 131.6, 125.6, 125.2, 121.2, 120.4, 119.6, 118.2, 74.8, 52.0, 48.5, 34.6, 34.5, 12.8.MS *m*/*z* (%): 423.19 (M^+, 22.65).

2.1.3.6. (E)-N-(4-Ethoxyphenyl)-2-(1′-methylspirochroman-2,4′-piperidin-4-ylidene)hydrazine carboxamide (5g). White solid; (83%). M.p. 220–222 °C. IR (νmax/cm^{-1}): 3375, 3210 (NHs), 3104, 2935 (CHs), 1679 (C=O), 1597, 1210, 1130. ^{1}H NMR (400 MHz, DMSO d_6) δ 9.85 (s, 1H), 8.85 (s, 1H), 8.30 (dd, *J* = 7.9, 1.4 Hz, 1H), 7.53 (d, *J* = 9.0 Hz, 2H), 7.33 – 7.23 (m, 1H), 6.97 (t, *J* = 7.5 Hz, 1H), 6.92 – 6.88 (m, 3H), 3.75 (s, 3H), 2.84 (s, 2H), 2.50 – 2.40 (m, 2H), 2.32 (t, *J* = 9.3 Hz, 2H), 2.21 (s, 3H), 1.78 (d, *J* = 13.5 Hz, 2H), 1.65 (t, *J* = 9.3 Hz, 2H). ^{13}C NMR (100 MHz, DMSO d_6) δ 155.5, 154.3, 154.1, 139.9, 132.4, 131.2, 125.4, 122.7, 121.2, 120.7, 118.1, 114.1, 74.1, 55.7, 50.9, 46.2, 34.6, 34.5.MS *m*/*z* (%): 394.88 (M^+, 34.49).

2.1.3.7. (E)-2-(1′-Ethylspirochroman-2,4′-piperidin-4-ylidene)-N-(4-methoxyphenyl)hydrazine carboxamide (5h). White solid; (85%). M.p. 230–232 °C. IR (νmax/cm^{-1}): 3375, 3203 (NHs), 3100, 2940 (CHs), 1678 (C=O), 1597, 1540, 1108. ^{1}H NMR (400 MHz, DMSO d_6) δ 9.85 (s, 1H), 8.85 (s, 1H), 8.30 (d, *J* = 6.8 Hz, 1H), 7.53 (d, *J* = 8.9 Hz, 2H), 7.27 (dd, *J* = 11.1, 4.2 Hz, 1H), 6.96 (t, *J* = 7.6 Hz, 1H), 6.92 – 6.88 (m, 3H), 3.75 (s, 3H), 2.84 (s, 2H), 2.53 (s, 2H), 2.37 (q, *J* = 7.1 Hz, 2H), 2.34 – 2.29 (m, 2H), 1.79 (d, *J* = 13.5 Hz, 2H), 1.63 (t, *J* = 9.8 Hz, 2H), 1.01 (t, *J* = 7.1 Hz, 3H). ^{13}C NMR (100 MHz, DMSO d_6) δ 155.5, 154.3, 154.2, 139.9, 132.4, 131.2, 125.4, 122.7, 121.1, 120.7, 118.1, 114.1, 74.7, 55.7, 52.0, 48.5, 34.6, 34.5, 12.8.MS *m*/*z* (%): 408.95 (M^+, 13.06).

2.1.3.8. (E)-2-(1′-Methylspirochroman-2,4′-piperidin-4-ylidene)-N-(4-methyl phenyl)hydrazine carboxamide (5i). White solid; (77%). M.p. 248–250 °C. IR (νmax/cm^{-1}): 3365, 3213 (NHs), 3104, 2940 (CHs), 1675 (C=O), 1597, 1530, 1128. ^{1}H NMR (400 MHz, DMSO d_6) δ 9.89 (s, 1H), 8.87 (s, 1H), 8.28 (d, *J* = 7.8 Hz, 1H), 7.54 (d, *J* = 8.2 Hz,

2H), 7.29 (t, *J* = 7.6 Hz, 1H), 7.13 (d, *J* = 8.2 Hz, 2H), 6.97 (t, *J* = 7.5 Hz, 1H), 6.89 (d, *J* = 8.2 Hz, 1H), 2.84 (s, 2H), 2.47 (d, *J* = 11.0 Hz, 2H), 2.33 (d, *J* = 9.9 Hz, 2H), 2.28 (s, 3H), 2.21 (s, 3H), 1.78 (d, *J* = 13.3 Hz, 2H), 1.64 (t, *J* = 9.9 Hz, 2H). ^{13}C NMR (100 MHz, DMSO d_6) δ 154.2, 154.0, 140.1, 136.9, 131.9, 131.3, 129.3, 125.4, 121.2, 120.7, 120.6, 118.2, 74.1, 50.9, 46.2, 34.5, 34.5, 20.9.MS *m*/*z* (%): 378.45 (M^+, 19.55).

2.1.3.9. (E)-2-(1′-Ethylspirochroman-2,4′-piperidin-4-ylidene)-N-(4-methyl phenyl)hydrazine carboxamide (5j). White solid; (75%). M. p. 223−225 °C. IR (*v*max/cm^{-1}): 3340, 3211 (NHs), 3104, 2900 (CHs), 1679 (C═O), 1597, 1538, 1156. ^{1}H NMR (400 MHz, DMSO d_6) δ 9.90 (s, 1H), 8.88 (s, 1H), 8.28 (d, *J* = 6.9 Hz, 1H), 7.54 (d, *J* = 8.3 Hz, 2H), 7.28 (dd, *J* = 11.2, 4.2 Hz, 1H), 7.11 (d, *J* = 8.3 Hz, 2H), 6.97 (t, *J* = 7.4 Hz, 1H), 6.89 (d, *J* = 8.1 Hz, 1H), 2.84 (s, 2H), 2.53 (s, 2H), 2.37 (q, *J* = 7.1 Hz, 2H), 2.34 – 2.29 (m, 2H), 2.28 (s, 3H), 1.79 (d, *J* = 13.1 Hz, 2H), 1.64 (d, *J* = 9.8 Hz, 2H), 1.01 (t, *J* = 7.1 Hz, 3H). ^{13}C NMR (100 MHz, DMSO d_6) δ 154.2, 154.0, 140.1, 136.9, 131.9, 131.3, 129.3, 125.4, 121.2, 120.6, 118.7, 118.2, 74.7, 52.0, 48.5, 34.6, 34.5, 20.9, 12.8.MS *m*/*z* (%): 392.30 (M^+, 26.05).

2.2. Biological evaluation

2.2.1. In vitro antiproliferative study against MCF-7, HCT-116, MCF-7, PC3 and A549 cell lines

The MTT assay was performed to evaluate the in vitro antiproliferative activity of the newly synthesized compounds according to the reported method using MCF-7, HCT-116, MCF-7, PC3 and A549 cancer cell lines (Denizot and Lang, 1986).

2.2.2. In vitro cytotoxic activity of all synthesized compounds against WI-38 cell line

The cytotoxicity of compounds **5a** and **5 g** was estimated according to the reported procedure (El-Azab et al., 2023, Al-Sanae et al., 2023).

2.2.3. In vitro enzyme inhibitory assays (against EGFR and Her-2)

Enzyme inhibitory assays for the most active compounds **5a**,**5b** and **5 g** were performed as described in the previous reports (El-Azab et al., 2020; Abdel-Aziz, et al., 2021).

2.2.4. Flow cytometry analysis of the cell cycle distribution

Cell cycle analysis was performed using different cancer cell lines stained with propidium iodide (PI) and FACS Calibur flow cytometer as previously described (Ormerod, 2002; Mosmann, 1983; Othman et al., 2023).

2.2.5. Cellular apoptosis analysis

Apoptosis was induced using an annexin 5-FITC/PI detection kit, as previously reported (Vermes, et al., 1995; Kumar et al., 2021; Hamdi et al., 2022a, 2022b; Al-Warhi et al., 2020).

2.3. Molecular docking and ADME methodology

Molecular docking methodology was performed using a well-established and reported protocols (Hamdi et al., 2022a, 2022b; Al-Suwaidan et al., 2015; Goda et al., 2005; El-Ayaan et al., 2007). ADME online tools were used to predict the pharmacokinetic, physicochemical, and drug-likeness properties of the target compounds (Lipinski et al., 2001; Hughes et al., 2008; Gleeson, 2008; Johnson et al., 2009).

3. Results

3.1. Chemistry

Scheme 1 outlines the synthesis of the targeted spirochromane compounds **4a-e** and **5a-j**. The starting materials, spirochromanones**2a**,**b**, were prepared using Kabbe's multicomponent reaction, which involved the thermal condensation of *N*-methylpiperidin-4-one or *N*-ethylpiperidin-4-onewith 2-hydroxyacetophenone, and pyrrolidine in methanol (Battisti et al., 2014; Abdelatef et al., 2018).Compounds **2a** and 2**b** were reacted with hydrazine hydrate in ethanol at room temperature to afford the corresponding hydrazineylidene spirochromane intermediates **3a** and **3b**, which were used directly in the subsequent steps without further purification. The final Schiff's bases **4a-e** were prepared by refluxing derivatives **3a** and **b** with the appropriate aldehyde in ethanol, using glacial acetic acid as a catalyst. Finally, compounds **5a-j** were obtained by coupling the properhydrazineylidenespirochromane **3a**,**b** with various phenyl isocyanates to furnish them with reliable yields. All synthesized structures of the final novel spirochromane compounds were confirmed by NMR, IR and MS (Supplementary data). Overall, the ^{1}-HNMR spectra of all the final newderivatives revealed the disappearance of two amine protons related to the NH_2 group of hydrazineylidenespirochromane derivatives **3a** and **3b**, which usually appeared as a singlet peak near 5.31 ppm. The ^{1}HNMR spectra of Schiff's bases **4a-e** showed a singlet proton around 8.48 ppm relative to the benzylidene proton (—CH═N—). Also, derivatives **5a-j** showed the appearance of two singlet protons near 8.95 and 9.93 ppm, assigned to the two protons of urea (HN-CO-NH) moiety.

Moreover, the ^{13}CNMRspectra of products **4a-e** and **5a-j** showed characteristic aliphatic peaks near 75.0, 51.0 and 36.0 ppm, corresponding to methylene groups of the spirochromane system. Besides, compounds **5a-j** exhibited a distinct peak at approximately 154.0 ppmassigned to the carbonyl group of urea fragment. IR spectrum revealed characteristic peaks near 3300 cm^{-1} regions relative to the amino groups of urea moiety.

3.2. Biological activity

3.2.1. In vitro antiproliferative activity

The newly synthesized compounds **4a-e** and **5a-j** were screened for their antiproliferative activity against breast adenocarcinoma (MCF-7), human colon carcinoma (HCT-116), human prostate cancer (PC3) and human lung adenocarcinoma (A549) cells at various concentrations *via* the standard MTT assay method using Doxorubicin (DOX) and Afatinib as reference drugs (Table 1) (Denizot and Lang, 1986; Hamdi et al., 2022a, 2022b). Among the tested compounds, derivatives **4a** and **5a-c** showed the most potent antiproliferative activity against the four cancer cell lines with an IC_{50} range of 1.673–13.47 μM. Besides, compounds **4d** and **5g** showed strong antiproliferative activity against MCF-7, HCT-116, and PC3 (IC_{50} values range of 1.154–10.08 μM) and moderate activity against A549 with IC_{50} values of 23.20 and 29.36 μM, respectively.

In derivatives **4a-e**, compound **4b** exhibited moderate activity against MCF-7, HCT-116 and A549 with IC_{50} values of 26.43, 31.02, and 42.54 μM, respectively. However, a weak PC3 antiproliferative activity with IC_{50} of 59.25 μM was observed. In addition, compound **4e** exerted moderate antiproliferative activity against the four cancer cell lines with an IC_{50} range of 20.62–49.45 μM. Derivative **4c** possessed moderate A549 antiproliferative activity with an IC_{50} value of 48.53 μM and weak activity against all other cancer cell lines. Among the **5a-j** series, compound **5i** showedextreme activity against HCT-116, PC3 and A549 with IC_{50} values of

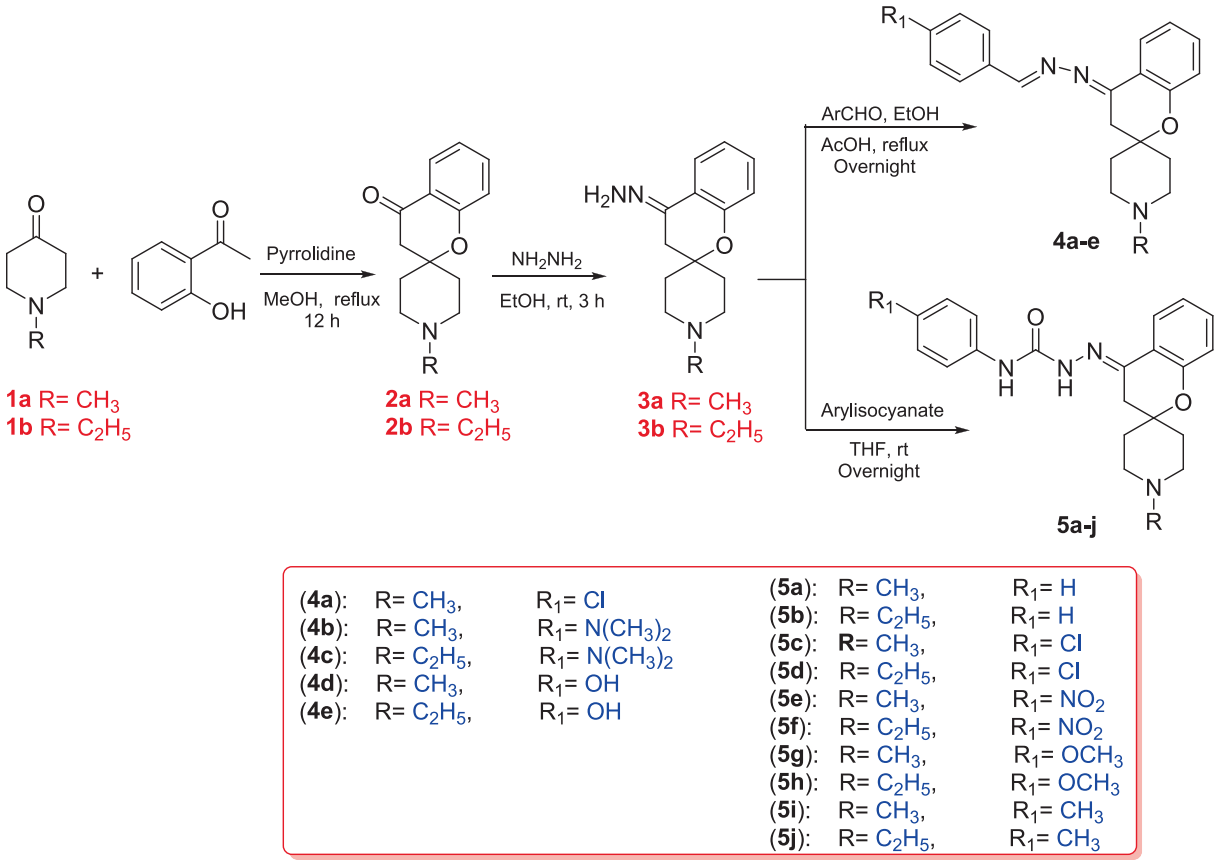

Scheme 1. Synthesis of the target spirochromanes **4a-e** and **5a-j**.

Table 1
In vitro antiproliferative study (IC_{50} values μM) of the final target compounds **4a-e** and **5a-j** against four cancer cell lines and WI38 normal cell line, in comparison with DOX and Afatinib.

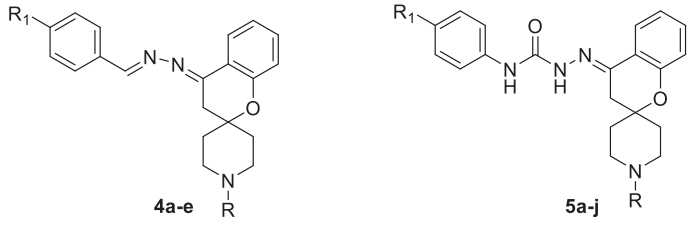

Comp. No.	R	R_1	*In vitro* Cytotoxicity IC_{50} (μM)[a]				
			MCF7	HCT-116	PC3	A549	WI38
4a	CH_3	Cl	8.74 ± 0.42	13.47 ± 0.57	12.71 ± 0.49	2.026 ± 0.09	75.71 ± 4.3
4b	CH_3	$N(CH_3)_2$	26.43 ± 1.27	31.02 ± 1.32	59.25 ± 2.28	42.54 ± 1.91	60.35 ± 3.7
4c	C_2H_5	$N(CH_3)_2$	79.98 ± 3.83	56.20 ± 2.39	55.04 ± 2.12	48.53 ± 2.18	55.30 ± 3.3
4d	CH_3	OH	10.08 ± 0.48	2.68 ± 0.11	2.371 ± 0.09	23.20 ± 1.04	33.26 ± 2.3
4e	C_2H_5	OH	35.55 ± 1.51	49.45 ± 2.1	22.2 ± 0.86	20.62 ± 0.93	47.53 ± 2.9
5a	CH_3	H	1.673 ± 0.07	5.602 ± 0.24	12.33 ± 0.48	5.827 ± 0.26	49.62 ± 3.0
5b	C_2H_5	H	6.033 ± 0.27	2.991 ± 0.13	9.09 ± 0.35	1.904 ± 0.09	65.6 ± 2.7
5c	CH_3	Cl	2.904 ± 0.11	2.575 ± 0.13	2.56 ± 0.13	8.029 ± 0.36	100
5d	C_2H_5	Cl	23.58 ± 0.92	21.74 ± 0.88	27.22 ± 1.05	47.67 ± 2.14	100
5e	CH_3	NO_2	10.85 ± 0.42	20.74 ± 0.88	19.15 ± 0.74	71.46 ± 3.21	67.22 ± 3.9
5f	C_2H_5	NO_2	56.79 ± 2.21	62.74 ± 2.67	11.33 ± 0.44	21.73 ± 0.98	57.46 ± 2.4
5 g	CH_3	OCH_3	6.674 ± 0.28	1.154 ± 0.05	3.302 ± 0.13	29.36 ± 1.32	72.93 ± 4.2
5 h	C_2H_5	OCH_3	38.95 ± 1.72	19.74 ± 0.84	15.51 ± 0.6	24.05 ± 1.08	83.47 ± 4.6
5i	CH_3	CH_3	21.43 ± 0.91	7.75 ± 0.33	9.71 ± 0.37	5.129 ± 0.23	66.27 ± 3.7
5j	C_2H_5	CH_3	18.99 ± 0.84	21.31 ± 0.91	5.47 ± 0.21	11.91 ± 0.53	100
Afatinib	–	–	5.10 ± 0.31	10.01 ± 0.47	7.98 ± 0.37	8.09 ± 0.69	49.50 ± 2.5
DOX	–	–	4.50 ± 0.2	5.23 ± 0.3	4.17 ± 0.2	5.57 ± 0.4	6.72 ± 0.5

[a] IC_{50} value is the concentration of compound that inhibits 50% of the cancer cell growth after 48 h of drug exposure as obtained from the MTT assay. Each value was shown as mean ± SD of three experiments. Bolded values represent the most potent antiproliferative derivatives.

7.75, 9.71 and 5.12 μM, respectively, whereas it showed moderate effect against MCF-7 with IC_{50} values of 21.43 μM. Also, derivative **5j** revealed extreme activity against PC3 with an IC_{50} value of 5.47 μM and potent activity against A549, MCF-7 and HCT-116 with IC_{50} values of 11.91, 18.99 and 21.31 μM in succession.Compound **5d** exhibited moderate antiproliferative activity against the four cancer cell lines with an IC_{50} range of 21.74–47.67 μM, while compound **5e** offered moderate activity against MCF-7, HCT-116 and PC3 (IC_{50} range of 10.85–20.74 μM) and weak inhibitory effect against A549. Besides, compound **5f** exerted strong cytotoxic activity against PC3 (IC_{50} = 11.33 μM) and A549 (IC_{50} = 21.73 μM) but showed weak activity against MCF-7 (IC_{50} = 56.79 μM) and HCT-116 (IC_{50} = 62.74 μM) cells. Compound **5 h** revealed vigorous activity against PC3 and HCT-116 cells with IC_{50} values of 15.51 and 19.74 μM in succession but showed moderate activity against A549 and MCF-7 with IC_{50} values of 24.05 and 38.95 μM, respectively.

3.2.2. In vitro cytotoxicity against normal human cell

A normal fibroblast-like fetal lung cell line (WI-38) was used further to investigate the therapeutic safety of the newly synthesized hybrids and evaluate their selective cytotoxicity displayed toward normal and tumour cells (El-Azab et al., 2023). DOX and Afatinib were used as the standard anticancer drugs for comparison (Table 1).

3.2.3. In vitro enzyme inhibition assays

The effect of the potent compounds **5a**, **5b** and **5 g** was screened against two molecular targets, EGFR and HER2 (El-Azab et al., 2020). These compounds showed reasonable inhibitory activity against both EGFR and HER-2 compared with the reference drugs, as shown in Table 2.

3.2.4. Cell cycle analysis

To obtain more detailed information regarding the mechanism of compounds **5a**, **5b** and **5g** regarding cancer cell growth inhibition, cell cycle distribution analysis and apoptosis induction (Fig. 3 and Table 3) were assessed using a propidium iodide (PI) staining assay (Ormerod, 2002; Mosmann, 1983; Othman et al., 2023).

3.2.5. Apoptosis detection

The percentage of apoptosis induced by compounds **5a**, **5b** and **5 g** was evaluated using an Annexin V-FITC/propidium iodide double-staining flow cytometry assay (Vermes, et al., 1995; Kumar et al., 2021; Hamdi et al., 2022a, 2022b) (Fig. 4 and Table 4).

3.3. In silico study

Molecular modeling is an important method for studying the physicochemical, pharmacokinetic and biological activities of bioactive molecules (Goda et al., 2005; El-Ayaan et al., 2007). In addition, it is used to explore the interactionsof ligands within the receptor- or putative enzyme-binding sites (Al-Suwaidan et al., 2015; Alanazi et al., 2016). The selected compounds and co-crystallized inhibitors were subjected to molecular docking at the protein-binding sites to ensure docking accuracy and validation (Hamdi et al., 2022a, 2022b; Abuelizz et al., 2023).

3.3.1. Molecular docking of compounds 5a, 5b and 5 g with EGFR and HER2

Compounds **5a**, **5b** and **5g** were dockedinto the binding siteof the EGFR, along with a co-crystallized bound inhibitor, to investigate the orientation and binding affinity of these compounds to the allosteric site of EGFR (Fig. 5, Fig. S1 and Table S1). The crystal 3D structure of EGFR and its bound inhibitor were obtained from PDB (PDB code: 7jxq) (Nicholson et al., 2001). Similarly, the 3D crystal structure of HER2 co-crystallized with its bound inhibitor was retrieved from PDB (PDB code: 7JXH) (Fig. 6, Fig. S2 and Table S2) (Son et al., 2022).

3.3.2. Pharmacokinetic and physicochemical predictions

The pharmacokinetic and physicochemical properties of the most active compounds **5a**, **5b** and **5 g** were predicted using the automated ADMETlab 2.0 web server (https://admetmesh.scbdd.com/) online calculation system (Table S3). Compounds **5a**, **5b** and **5 g** demonstrated varying characteristics based on the drug-likeness and ADMET properties evaluation (Lipinski et al., 2001; Hughes et al., 2008; Gleeson, 2008; Johnson et al., 2009).

Table 2
In vitro EGFR-2, and Her-2 inhibitory effects of the synthesized compounds **5a**, **5b** and **5 g**.

Comp. No.	IC_{50} (μM)[a]	
	EGFR Inhibition	Her2 Inhibition
5a	0.116 ± 0.005	0.055 ± 0.003
5b	0.132 ± 0.006	0.21 ± 0.01
5 g	0.077 ± 0.004	0.085 ± 0.004
Erlotinib	0.09 ± 1.65	0.038 ± 0.002
Gefitinib	0.052 ± 0.78	0.072 ± 0.98

[a] IC_{50} value is the compound concentration required to produce 50% inhibition.

4. Discussion

Structure-activity relationship (SAR) analysis of the antiproliferative activity of the newly synthesized compounds against MCF-7, HCT-116, PC3 and A549 cells generally revealed that 1′-methyl-4-hydrazono spirochromane-2,4′-piperidines (**4a**, **4b**, **4d**, **5a**, **5c**, **5e**, **5 g** and **5i**) showed improved activity compared to 1′-ethyl-4-hydrazono spirochromane-2,4′-piperidines (**4c**, **4e**, **5b**, **5d**, **5f**, **5 h** and **5j**). In addition, compounds **5a-j**, with a hydrazine carboxamide moiety as a long linker, exhibited slightly better antiproliferative activity than arylidene incorporating derivatives **4a-e**. Of the arylidene derivatives **4a-e**, the best activity was from 4-chloro and 4-hydroxylbenzylidene derivatives **4a** and **4d**, which showed reliable antiproliferative activity against the four cancer cell lines with IC_{50} range of 2.02–23.20 μM. However, the less potent derivative among this series is ethyl piperidine derivative **4c**, having 4-dimethylamino substituent with an IC_{50} range of 48.53–79.98 μM against all cancer cell lines.

As for the hydrazine carboxamide derivatives **5a-j**, the results revealed that compounds containing unsubstituted phenyl moieties, such as compounds **5a** and **5b**, exhibited powerful antiproliferative activity against all tested cancer cell lines with IC_{50} range of 1.67–12.33 μM. Furthermore, the substitution of the phenyl moieties had a remarkable effect. Except for compound **5c**, electron-donating groups notably enhanced the antiproliferative activity, as in compound **5 g** substituted with a methoxy group and compound **5i** substituted with amethyl group. These compounds exhibited activity ranging from very strong to moderate effect against all cancer cell lines (IC_{50} range of 1.154–29.36 μM). Besides, *N*-ethyl piperidine incorporating derivatives as compounds **5h** and **5j**, substituted with methoxy and methyl groups in success, showed remarkable antiproliferative activity against all tested cancer cell lines with IC_{50} values range of 5.47–38.95 μM.

In contrast, *N*-methylpiperidine derivative **5c** with a 4-chloro phenyl fragment showed extreme antiproliferative activity against all tested cancer cell lines with an IC_{50} range of 2.575–8.029 μM. In contrast, *N*-ethylpiperidine derivative **5d** with the same 4-chloro

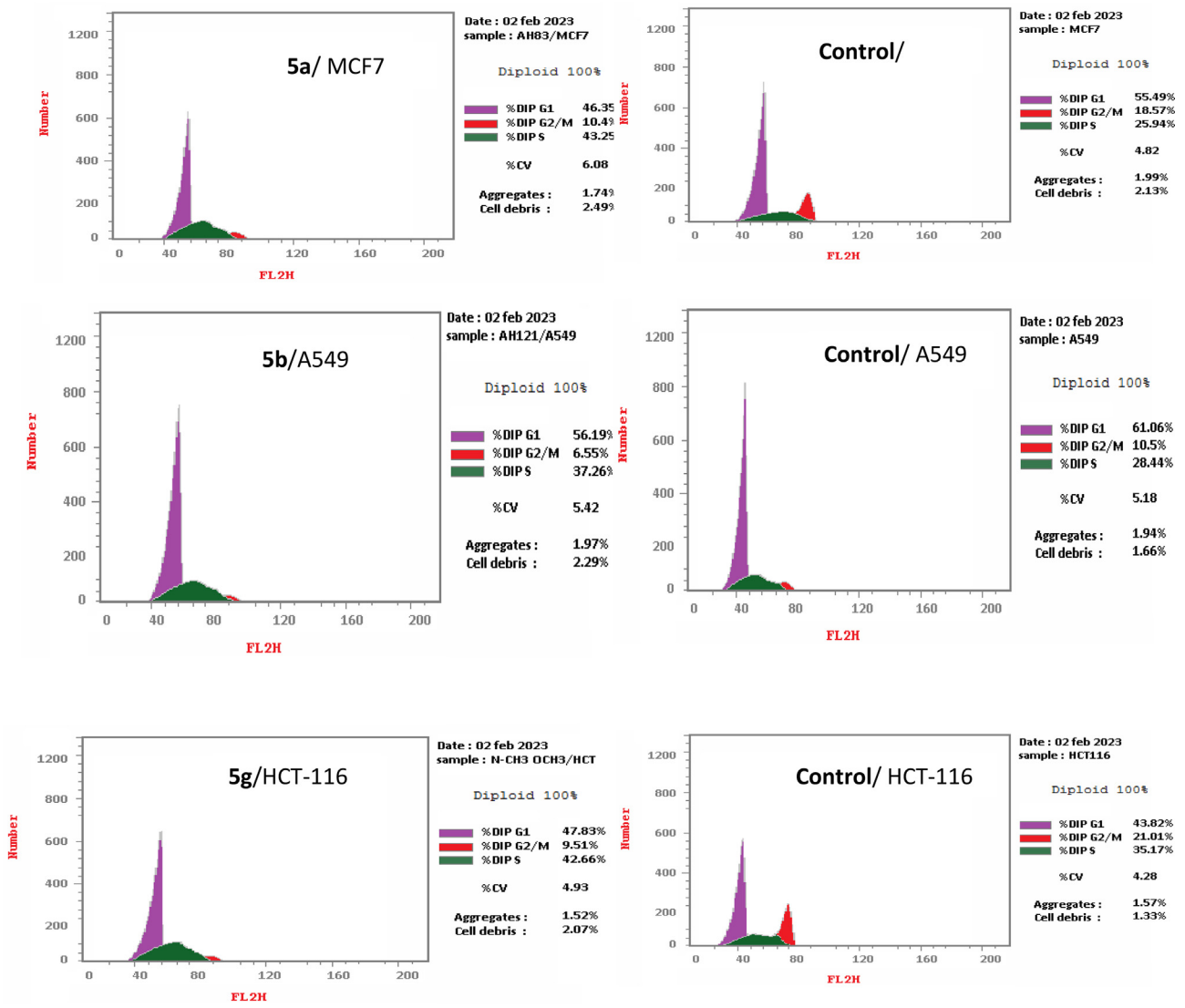

Fig. 3. Flow cytometry analysis of DNA ploidy in different cancer cells after treatment with compounds **5a**, **5b** and **5g.**

Table 3
Effect of compounds **5a**, **5b** and **5 g** on the cell cycle distribution in different cancer cell lines.

Comp. No.	Cell cycle distribution (%)		
	%G_0-G_1	%S	%G_2/M
5a/MCF7	46.35	43.25	10.4
Cont.MCF7	55.49	25.94	18.57
5b/A549	56.19	37.26	6.55
Cont. A549	61.06	28.44	10.5
5 g/HCT-116	47.83	42.66	9.51
Cont. HCT-116	43.82	35.17	21.01

phenyl moiety displayed a moderate antiproliferative effect against the four cell lines with an IC_{50} range of 21.74–47.67 μM. Finally, *N*-methylpiperidine derivative **5e** incorporating 4-nitro phenyl group exhibited a strong effect against MCF7, HCT-116, and PC3 with IC_{50} values of 10.85, 20.74 and 19.15 μM, respectively, while it showed a weak effect against A549 with $IC_{50}$of 71.46 μM. Also, *N*-ethylpiperidine derivative **5f** with nitrophenyl moiety exhibited strong activity against PC3 (IC_{50} = 11.33 μM) and A549 (**IC_{50}** = 21.73 μM), whereas it showed weak activity against the other two cell lines MCF7 (IC_{50} = 56.79 μM) and HCT-116 (IC_{50} = 62.74 μM).

As shown in Table 1, the investigated compounds exhibited lower cytotoxicity against normal fibroblast cells WI-38 as denoted from their IC_{50} values with the range of 33.26–100 μM, proving that they have substantially better results than DOX and Afatinib on normal cells. Notably, derivatives **4a**, **4d**, **5a**, **5b**, **5c**, **5 g**, **5i** and **5j** induced lower toxic effects on WI-38 cells, with IC_{50} values of 75.71, 33.26, 49.62, 65.6, 100, 72.93, 66.27 and 100 μM, respectively, compared with that by DOX (IC_{50} = 6.72 μM) and Afatinib (IC_{50} = 49.50 μM).

In enzyme inhibition assay, the newly synthesized spirochromane derivative **5a** showed a vigorous inhibitory activity against HER2 (IC_{50} = 0.055 μM) compared with Gefitinib (IC_{50} = 0.072 μM). In addition, derivative **5 g** showed more vigorous EGFR inhibitory activity (IC_{50} = 0.077 μM), compared to that of Erlotinib (IC_{50} = 0.09 μM) (Table 2).

On the other hand, cell cycle distribution results (Fig. 3 and Table 3) revealed that compound **5a** induced apoptosis in the G_0-G_1 phase in 46.35% of MCF7 cells, whereas untreated cells showed 55.49% apoptosis. Also, derivative **5b** induced apoptosis in the G_0-G_1 phase by 56.19 % in A549 cells, whereas untreated cells showed 61.06 % apoptosis. In addition, compound **5 g** induced apoptosis in

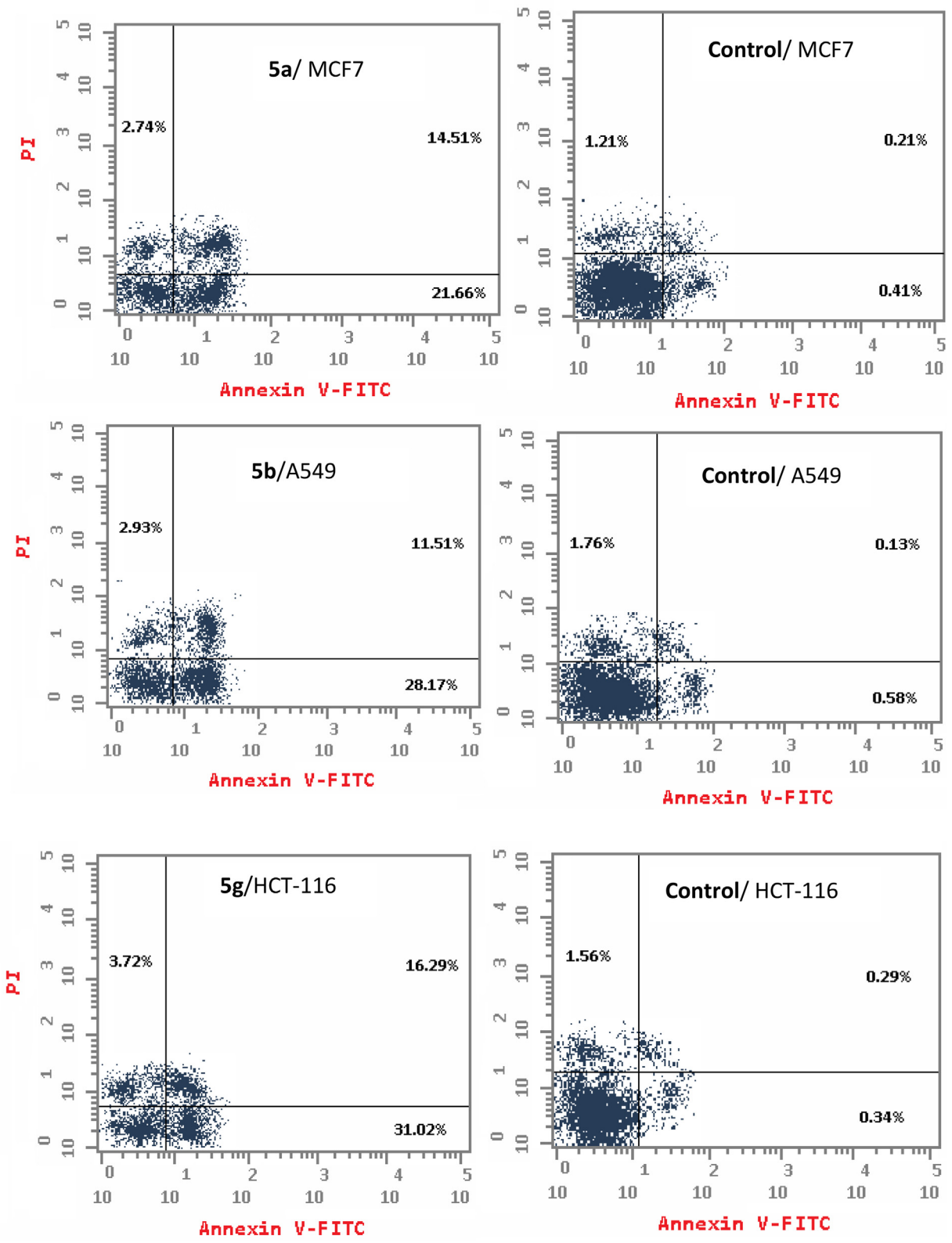

Fig. 4. Effect of compounds **5a**, **5b** and **5g** on the percentage of Annexin V-FITC-positive staining. The cells were treated with DMSO as a control, **5a**, **5b** and **5g** for 24 h.

the G_0-G_1 phase in 47.83% of HCT-116 cells, whereas untreated cells showed 43.82% apoptosis. In the S phase, derivative **5a** showed a high apoptotic effect (43.25%) compared to the untreated MCF7 cells (25.94%). Compound**5b** exhibited 37.26% apoptotic effect in comparison with untreated A549 cells (28.44%). Moreover, derivative **5 g** showed a strong apoptotic effect (42.66%) compared to the untreated HCT-116 cells (35.17%). In the G_2/M phase, compounds **5a**, **5b** and **5 g** showed 10.4%, 6.55 % and9.51% apoptotic

Table 4
Total apoptosis (early, late) and necrosis induction analysis induced by compounds **5a**, **5b** and **5g,** compared to control.

Comp. No.	Apoptosis			Necrosis
	Total	Early	Late	
5a/MCF7	36.17	21.66	14.51	2.74
Cont.MCF7	0.62	0.41	0.21	1.21
5b/A549	39.68	28.17	11.51	2.93
Cont. A549	0.71	0.58	0.13	1.76
5g/HCT-116	47.31	31.02	16.29	3.72
Cont. HCT-116	0.63	0.34	0.29	1.56

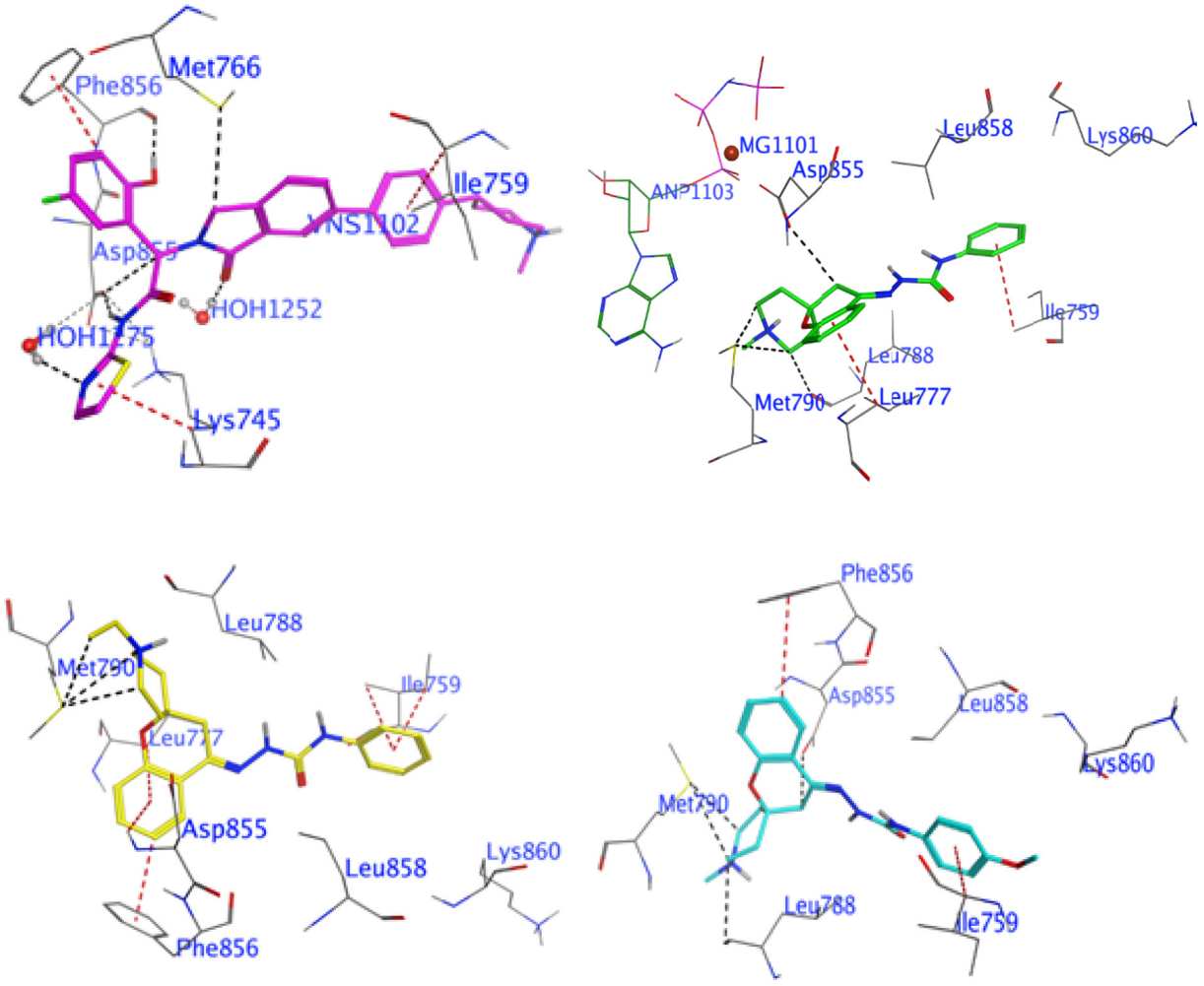

Fig. 5. The 3D interaction profiles and best interaction poses of investigated compounds placed into the EGFR (7jxq) by docking study: co-crystallized inhibitor (upper left panel), **5a** (upper right panel), **5b** (lower left panel), and **5g** (lower right panel).

effect, respectively, whereas control cells showed 18.59%, 10.5% and 21.01% inhibition. Thus, compounds **5a**, **5b** and **5g** arrested cell growth inthe S phase.

According to apoptosis detection, as shown in Fig. 4 and Table 4, compounds **5a**, **5b** and **5 g** induced early apoptosis after 24 h incubation by 21.66% (MCF**-7** cells), 28.17 % (A549cells) and 31.02% (HCT-116cells), respectively, whereas the untreated cells induced early apoptosis by approximately 0.34–0.58%.

In addition, the tested compounds **5a**, **5b** and **5 g** enhanced the late apoptotic induction by 14.51%, 11.51 and 16.29%, in success, compared with that in the untreated control (0.13–0.29%). Furthermore, derivatives **5a**, **5b** and **5g** promoted cell necrosis by 2.74%, 2.93% and 3.72%, respectively, compared with untreated cells, which showed approximately 1.21–1.76%. Cumulatively, compounds **5a**, **5b** and **5 g** enhanced the total apoptosis by 36.17%, 39.68% and 47.31 %, respectively, compared with untreated cell (0.62–0.71%). In addition,the data support an apoptotic mechanism underlying the programmed cell death induced by compounds **5a**, **5b** and **5 g** rather than a necrotic pathway.

Molecular docking of compounds **5a**, **5b** and **5g** with EGFR revealed that EGFR allosteric inhibitors bound to EGFR at a site away from the tyrosine kinase domain, which passed the cysteine797 mediated resistance mechanism, demonstrating a promising strategy to overcome JBJ-09–063 resistance induced by

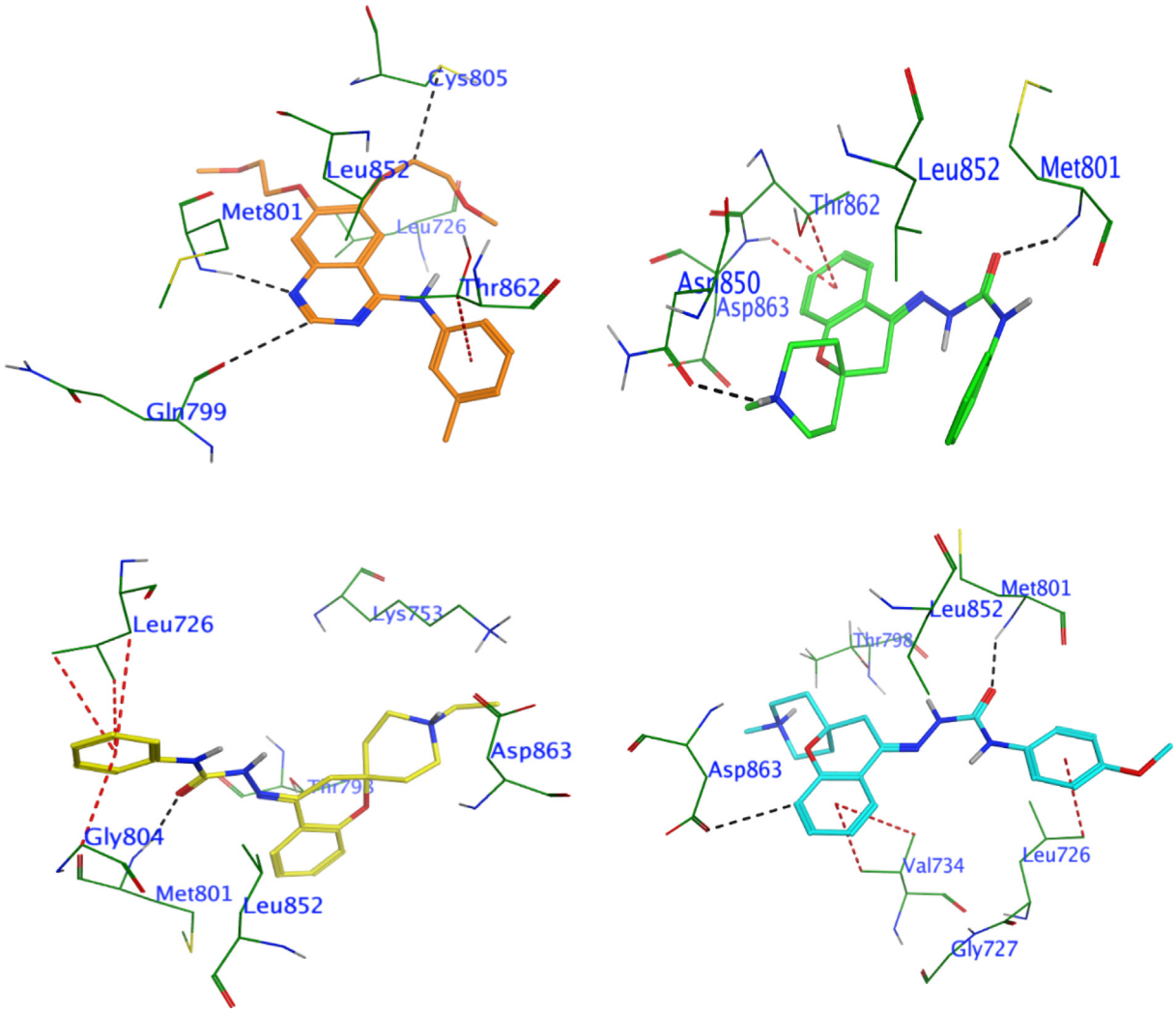

Fig. 6. The 3D interaction profiles and best interaction poses of investigated compounds placed into the Her2 (PDB ID: 7jxh) by docking study: co-crystallized inhibitor (upper left panel), **5a** (upper right panel), **5b** (lower left panel) and **5g** (lower right panel).

cysteine797s. The docking of the high-potency compound **5 g** with the EGFR resulted in a binding affinity of − 9.61 kcal/mol. Compound **5 g** interacted with the allosteric site of EGFR *via* four H-bond donors of the crucial amino acid residues ASP855, LEU788 and MET790, along with two π-H bonds with PHE856 and ILE759 (Fig. 5, Table S1). Whereas compound **5a** has a binding affinity of −8.99 kcal/mol and forms four strong H-bond donors with crucial amino acid residues MET790, LEU788 and ASP855, as well as two π-H bonds with LEU777 and ILE759 (Fig. 5, Table S1). Additionally, compound **5b** possesses a binding affinity of −9.00 kcal/mol and interacts through three H-bond with main residue MET790 in the allosteric site of EGFR, besides five π-bond with amino acid residues PHE856, ILE759, LEU777 and ASP855 (Fig. 5, Table S1). Furthermore, Figure S1 shows the alignment of the co-crystalline ligand with the investigated compounds (**5a**, **5b** and **5 g**),which interact with identical residues as the co-crystalline ligand in the allosteric site.

Similarly, molecular docking of compounds **5a**, **5b** and **5g** to the HER2-binding cavity revealed that compounds **5g** and **5a** demonstrated high binding affinities, whereas compound **5b** showed moderate binding affinity. The docking simulation implied that the urea group in all investigated molecules (**5g**, **5a** and **5b**) was superimposed on the isatin group of the bound inhibitor within the hydrophobic binding pocket of HER2 (Fig. 6, Table S2). Moreover, the carbonyl group on the urea part of molecules **5a**, **5b** and **5g** formed hydrogen bonds with the curial amino acid residue MET 801, which supported that these compounds may inhibit the same target enzyme asa co-crystallized inhibitor. In addition, compound **5g** made two H-bond donors with THR798 and ASP863 and an H-bond acceptor with MET 801, as well as three π-bonds with LEU726 and VAL734, while compound **5a** formed two H-bonds with curial residues MET 801 and ASN 850, beside π-bond with ASP 863 (Fig. 6, Table S2). Compound **5b** interacted through two H-bonds with the curial residues MET801 and LYS753, in addition to three π-bonds with GLY804, MET801 and LEU726. The binding modes of compounds **5a**, **5b** and **5g** were similar to those of the co-crystallized bound inhibitor with HER2 kinase, as shown in the overlay protocol (Figure S2).

The pharmacokinetic and physicochemical properties of compound **5a** show good drug-likeness, according to Lipinski, Pfizer, GSK, and Golden Triangle. It has moderate medicinal chemistry properties, limited absorption, high distribution, moderate metabolism, and moderate toxicity. In contrast,derivative **5b** exhibited good drug-likeness according to the Lipinski Rule and Golden Triangle but was rejected by the Pfizer and GSK Rules. It demonstrates moderate medicinal chemistry properties, limited absorption, limited distribution, moderate metabolism, and moderate toxicity. Also, derivative **5g** possesses good drug-likeness based on the Lip-

inski Rule, Pfizer Rule, and Golden Triangle. It exhibited moderate medicinal chemistry properties, limited absorption, low distribution, moderate metabolism, and moderate toxicity. Considering these factors, spirochromane derivative**5a** emerged as the best candidate owing to its favourable drug-likeness profile and moderate ADMET properties.The ADMET lab 2.0 web tool calculations of compounds **5a**, **5b** and **5g** predicted that they possessed appropriate pharmacokinetic and physicochemical properties (Table S3).

5. Conclusions

Two new series of spirochromanes **4a-e** and **5a-j** were synthesized and their antiproliferative activities were evaluated using four human cancer cell lines, i.e., MCF-7, HCT-116, PC3 and A549. Compounds **5b** and **5c** exhibited broad spectrum activity against the MCF-7 (IC_{50} of 6.03 and 2.90 μM, respectively), HCT-116 (IC_{50} of 2.99 and 2.575 μM, respectively), PC3 (IC_{50} of 9.09 and 2.56 μM, respectively) and A549 (IC_{50} of 1.90 and 8.029 μM, respectively) cell lines. Furthermore, derivatives **4d** and **5 g** showed broad spectrum activity against the MCF-7 (IC_{50} of 10.08 and 6.67 μM, respectively), HCT-116 (IC_{50} of 2.68 and 1.154 μM, respectively) and PC3 (IC_{50} of 2.37 and 3.30 μM, respectively) cell lines. Moreover, compound**5j** selectively inhibited the PC3 cell line with an IC_{50} value of 5.47 μM, while the MCF-7and A549 cell lines were selectively inhibited by derivative **4a** (IC_{50} of 8.74 and 2.026 μM, respectively). HCT-116, PC3 and A549 cell lines were strongly inhibited by derivative **5i** (IC_{50} of 7.75, 9.71, and 5.129 μM, respectively). Moreover, compound **5a** possessed potential antiproliferative activity against MCF-7, HCT-116 and A549 cell lines (IC_{50} of 1.67, 5.60 and 5.827 μM, respectively). The IC_{50} values of spirochromanes **4a-e** and **5a-j** were compared with those of the reference drugs Doxorubicin (IC_{50} range of 4.17–5.57 μM) and Afatinib (IC_{50} range of 5.10–10.01 μM).

The most active antiproliferative agents, **5a**, **5b** and **5g**, potently inhibited EGFR (IC_{50} = 0.116, 0.132, and 0.077 μM, respectively) and HER2 (IC_{50} = 0.055, 0.21 and 0.085 μM, respectively). The results were compared to the references Gefitinib (IC_{50} of 0.05 μM) and Erlotinib (IC_{50} of 0.038 μM). Cell cycle analysis and apoptosis detection data showed that compounds **5a**, **5b** and **5g** arrested cell growth inthe S phase, and the apoptotic mechanism was the main mechanism rather than the necrotic pathway. Docking studies of derivatives **5a**, **5b** and **5 g** into the putative binding sites of EGFR and HER2 were conducted to study the mode of interaction and requirements for antiproliferative activity. ADMETlab and drug-likeness predictions showed that compounds **5a**, **5b** and **5g** exhibited goodpharmacokinetic, physicochemical, and drug-likeness properties.

Declaration of competing interest

The authors declare that they have no known competing financial interests or personal relationships that could have appeared to influence the work reported in this paper.

Acknowledgements

The authors extend their appreciation to the Deputyship for Research & Innovation, "Ministry of Education" in Saudi Arabia, for funding this research (IFKSUOR3-435-1).

Appendix A. Supplementary material

Supplementary data to this article can be found online at https://doi.org/10.1016/j.jsps.2023.101803.

References

Abdelatef, S.A., El-Saadi, M.T., Amin, N.H., Abdelazeem, A.H., Omar, H.A., Abdellatif, K.R., 2018. Design, synthesis and anticancer evaluation of novel spirobenzo[h] chromene and spirochromane derivatives with dual EGFR and B-RAF inhibitory activities. Eur. J. Med. Chem. 150, 567–578.

Abdel-Aziz, A.-A.-M., El-Azab, A.S., AlSaif, N.A., Obaidullah, A.J., Al-Obaid, A.M., Al-Suwaidan, I.A., 2021. Synthesis, potential anti-tumor activity, cell cycle analysis, and multitarget mechanisms of novel hydrazones incorporating a 4-methylsulfonylbenzene scaffold: a molecular docking study. J. Enzyme Inhib. Med. Chem. 36 (1), 1521–1539.

Abdelsalam, E.A., Zaghary, W.A., Amin, K.M., Abou Taleb, N.A., Mekawey, A.A.I., Eldehna, W.M., Abdel-Aziz, H.A., Hammad, S.F., 2019. Synthesis and in vitro anticancer evaluation of some fused indazoles, quinazolines and quinolines as potential EGFR inhibitors. Bioorg. Chem. 89, 102985.

Abuelizz, H.A., Bakheit, A.H., Marzouk, M., El-Senousy, W.M., Abdellatif, M.M., Mostafa, G.A.E., Al-Salahi, R., 2023. Evaluation of some Benzo[g]Quinazoline derivatives as antiviral agents against human rotavirus wa strain: biological screening and docking study. Curr. Issues Mol. Biol. 45 (3), 2409–2421.

Alanazi, A.M., El-Azab, A.S., Al-Swaidan, I.A., Maarouf, A.R., El-Bendary, E.R., El-Enin, M.A.A., Abdel-Aziz, A.-A.-M., 2013. Synthesis, single-crystal, in vitro anti-tumor evaluation and molecular docking of 3-substitued 5,5-diphenylimidazolidine-2,4-dione derivatives. Med. Chem. Res. 22 (12), 6129–6142.

Alanazi, A.M., Abdel-Aziz, A.-A.-M., Shawer, T.Z., Ayyad, R.R., Al-Obaid, A.M., Al-Agamy, M.H., Maarouf, A.R., El-Azab, A.S., 2016. Synthesis, anti-tumor and antimicrobial activity of some new 6-methyl-3-phenyl-4(3H)-quinazolinone analogues: in silico studies. J. Enzyme Inhib. Med. Chem. 31 (5), 721–735.

Alkahtani, H.M., Abdalla, A.N., Obaidullah, A.J., Alanazi, M.M., Almehizia, A.A., Alanazi, M.G., Ahmed, A.Y., Alwassil, O.I., Darwish, H.W., Abdel-Aziz, A.-A.-M., El-Azab, A.S., 2020. Synthesis, cytotoxic evaluation, and molecular docking studies of novel quinazoline derivatives with benzenesulfonamide and anilide tails: Dual inhibitors of EGFR/HER2. Bioorg. Chem. 95, 103461.

Al-Sanea, M.M., Hamdi, A., Mohamed, A.A., El-Shafey, H.W., Moustafa, M., Elgazar, A. A., Eldehna, W.M., Ur Rahman, H., Parambi, D.G., Elbargisy, R.M., Selim, S., 2023. New benzothiazole hybrids as potential VEGFR-2 inhibitors: design, synthesis, anticancer evaluation, and in silico study. J. Enzyme Inhib. Med. Chem. 38 (1), 2166036.

Al-Suwaidan, I.A., Abdel-Aziz, N.I., El-Azab, A.S., El-Sayed, M.A., Alanazi, A.M., El-Ashmawy, M.B., Abdel-Aziz, A.-A.-M., 2015. Anti-tumor evaluation and molecular docking study of substituted 2-benzylidenebutane-1,3-dione, 2-hydrazonobutane-1,3-dione and trifluoromethyl-1H-pyrazole analogues. J. Enzyme Inhib. Med. Chem. 30 (4), 679–687.

Al-Suwaidan, I.A., Abdel-Aziz, A.-A.-M., Shawer, T.Z., Ayyad, R.R., Alanazi, A.M., El-Morsy, A.M., Mohamed, M.A., Abdel-Aziz, N.I., El-Sayed, M.-A.-A., El-Azab, A.S., 2016. Synthesis, anti-tumor activity and molecular docking study of some novel 3-benzyl-4(3H)quinazolinone analogues. J. Enzyme Inhib. Med. Chem. 31 (1), 78–89.

Al-Warhi, T., Abo-Ashour, M.F., Almahli, H., Alotaibi, O.J., Al-Sanea, M.M., Al-Ansary, G.H., Ahmed, H.Y., Elaasser, M.M., Eldehna, W.M., Abdel-Aziz, H.A., 2020. Novel [(N-alkyl-3-indolylmethylene)hydrazono]oxindoles arrest cell cycle and induce cell apoptosis by inhibiting CDK2 and Bcl-2: synthesis, biological evaluation and in silico studies. J. Enzyme Inhib. Med. Chem. 35 (1), 1300–1309.

Antonello, A., Tarozzi, A., Morroni, F., Cavalli, A., Rosini, M., Hrelia, P., Bolognesi, M.L., Melchiorre, C., 2006. Multitarget-directed drug design strategy: a novel molecule designed to block epidermal growth factor receptor (EGFR) and to exert proapoptotic effects. J. Med. Chem. 49 (23), 6642–6645.

Baker, S.J., Reddy, E.P., 2010. Targeted inhibition of kinases in cancer therapy. Mt Sinai J. Med. 77 (6), 573–586.

Barker, A.J., Gibson, K.H., Grundy, W., Godfrey, A.A., Barlow, J.J., Healy, M.P., Woodburn, J.R., Ashton, S.E., Curry, B.J., Scarlett, L., 2001. Studies leading to the identification of ZD1839 (Iressa™): an orally active, selective epidermal growth factor receptor tyrosine kinase inhibitor targeted to the treatment of cancer. Bioorg. Med. Chem. Lett. 11, 1911–1914.

Battisti, U.M., Corrado, S., Sorbi, C., Cornia, A., Tait, A., Malfacini, D., Cerlesi, M.C., Calo, G., Brasili, L., 2014. Synthesis, enantiomeric separation and docking studies of spiropiperidine analogues as ligands of the nociceptin/orphanin FQ receptor. MedChemComm 5, 973–983.

Bayat Mokhtari, R., Homayouni, T.S., Baluch, N., Morgatskaya, E., Kumar, S., Das, B., Yeger, H., 2017. Combination therapy in combating cancer. Oncotarget 8 (23), 38022–38043.

Black, J.D., Brattain, M.G., Krishnamurthi, S.A., Dawson, D.M., Willson, J.K., 2003. ErbB family targeting. Curr. Opin. Invest. Drugs 4, 1451–1454.

Christensen, J.G., 2007. A preclinical review of sunitinib, a multitargeted receptor tyrosine kinase inhibitor with anti-angiogenic and antitumour activities. Annal. Oncol.: Off. J. Eur. Soc. Medical Oncol. 18 (Suppl 10), x3–x.

Denizot, F., Lang, R., 1986. Rapid colorimetric assay for cell growth and survival: modifications to the tetrazolium dye procedure giving improved sensitivity and reliability. J. Immunol. Methods 89 (2), 271–277.

Dungo, R.T., Keating, G.M., 2013. Afatinib: first global approval. Drugs 73, 1503–1515.

El-Ayaan, U., Abdel-Aziz, A.-A.-M., Al-Shihry, S., 2007. Solvatochromism, DNA binding, anti-tumor activity and molecular modeling study of mixed-ligand copper(II) complexes containing the bulky ligand: bis[N-(p-tolyl)imino] acenaphthene. Eur. J. Med. Chem. 42 (11–12), 1325–1333.

El-Azab, A.S., Alanazi, A.M., Abdel-Aziz, N.I., Al-Suwaidan, I.A., El-Sayed, M.A., El-Sherbeny, M.A., Abdel-Aziz, A.-A.-M., 2013. Synthesis, molecular modeling study, preliminary antibacterial, and anti-tumor evaluation of N-substituted naphthalimides and their structural analogues. Med. Chem. Res. 22 (5), 2360–2375.

El-Azab, A.S., Al-Dhfyan, A., Abdel-Aziz, A.-A.-M., Abou-Zeid, L.A., Alkahtani, H.M., Al-Obaid, A.M., Al-Gendy, M.A., 2017. Synthesis, anticancer and apoptosis-inducing activities of quinazoline-isatin conjugates: epidermal growth factor receptor-tyrosine kinase assay and molecular docking studies. J. Enzyme Inhib. Med. Chem. 32 (1), 935–944.

El-Azab, A.S., Abdel-Aziz, A.-A.-M., Abou-Zeid, L.A., El-Husseiny, W.M., El Morsy, A.M., El-Gendy, M.A., El-Sayed, M.A., 2018. Synthesis, antitumour activities and molecular docking of thiocarboxylic acid ester-based NSAID scaffolds: COX-2 inhibition and mechanistic studies. J. Enzyme Inhib. Med. Chem. 33 (1), 989–998.

El-Azab, A.S., Abdel-Aziz, A.A., AlSaif, N.A., Alkahtani, H.M., Alanazi, M.M., Obaidullah, A.J., Eskandrani, R.O., Alharbi, A., 2020. Anti-tumor activity, multitarget mechanisms, and molecular docking studies of quinazoline derivatives based on a benzenesulfonamide scaffold: Cell cycle analysis. Bioorg. Chem. 104, 104345.

El-Azab, A.S., Alkahtani, H.M., AlSaif, N.A., Al-Suwaidan, I.A., Obaidullah, A.J., Alanazi, M.M., Al-Obaid, A.M., Al-Agamy, M.H.M., Abdel-Aziz, A.-A.-M., 2023. Synthesis, antiproliferative and enzymatic inhibition activities of quinazolines incorporating benzenesulfonamide: Cell cycle analysis and molecular modeling study. J. Mol. Struct. 127815, 134928.

El-Husseiny, W.M., El-Sayed, M.A., Abdel-Aziz, N.I., El-Azab, A.S., Asiri, Y.A., Abdel-Aziz, A.-A.-M., 2018. Structural alterations based on naproxen scaffold: Synthesis, evaluation of anti-tumor activity and COX-2 inhibition, and molecular docking. Eur. J. Med. Chem. 158, 134–143.

El-Sherbeny, M.A., Abdel-Aziz, A.-A.-M., Ahmed, M.A., 2010. Synthesis and anti-tumor evaluation of novel diarylsulfonylurea derivatives: molecular modeling applications. Eur. J. Med. Chem. 45 (2), 689–697.

Frampton, J.E., 2009. Lapatinib: a review of its use in the treatment of HER2-overexpressing, trastuzumab-refractory, advanced or metastatic breast cancer. Drugs 69, 2125–2148.

Fu, R.G., Sun, Y., Sheng, W.B., Liao, D.F., 2017. Designing multitargeted agents: An emerging anticancer drug discovery paradigm. Eur. J. Med. Chem. 136, 195–211.

George, R.F., 2018. Facile synthesis of simple 2-oxindole-based compounds with promising antiproliferative activity. Future Med. Chem. 10 (3), 269–282.

Gleeson, M.P., 2008. Generation of a set of simple, interpretable ADMET rules of thumb. J. Med. Chem. 51 (4), 817–834.

Goda, F.E., Abdel-Aziz, A.-A.-M., Ghoneim, H.A., 2005. Synthesis and biological evaluation of novel 6-nitro-5-substituted aminoquinolines as local anesthetic and anti-arrhythmic agents: molecular modeling study. Bioorg. Med. Chem. 13 (9), 3175–3183.

Gullick, W.J., 1991. Prevalence of aberrant expression of the epidermal growth factor receptor in human cancers. Br. Med. Bull. 47 (1), 87–98.

Gundla, R., Kazemi, R., Sanam, R., Muttineni, R., Sarma, J.A., Dayam, R., Neamati, N., 2008. Discovery of novel small-molecule inhibitors of human epidermal growth factor receptor-2: combined ligand and target-based approach. J. Med. Chem. 51, 3367–3377.

Hamdi, A., Said, E., Farahat, A., El-Bialy, S., Massoud, M., 2016. Synthesis and in vivo antifibrotic activity of novel leflunomide analogues. Lett. Drug Des. Discovery 13 (9), 912–920.

Hamdi, A., Elhusseiny, W.M., Othman, D.I., Haikal, A., Bakheit, A.H., El-Azab, A.S., Al-Agamy, M.H., Abdel-Aziz, A.-A.-M., 2022a. Synthesis, anti-tumor, and apoptosis-inducing activities of novel 5-arylidenethiazolidine-2,4-dione derivatives: Histone deacetylases inhibitory activity and molecular docking study. Eur. J. Med. Chem. 244, 114827.

Hamdi, A., El-Shafey, H.W., Othman, D.I., El-Azab, A.S., AlSaif, N.A., Abdel-Aziz, A.-A.-M., 2022b. Design, synthesis, anti-tumor, and VEGFR-2 inhibition activities of novel 4-anilino-2-vinyl-quinazolines: Molecular modeling studies. Bioorg. Chem. 122, 105710.

Holohan, C., Van Schaeybroeck, S., Longley, D.B., Johnston, P.G., 2013. Cancer drug resistance: an evolving paradigm. Nat. Rev. Cancer 13 (10), 714–726.

Housman, G., Byler, S., Heerboth, S., Lapinska, K., Longacre, M., Snyder, N., Sarkar, S., 2014. Drug resistance in cancer: an overview. Cancers 6 (3), 1769–1792.

Hughes, J.D., Blagg, J., Price, D.A., Bailey, S., Decrescenzo, G.A., Devraj, R.V., Ellsworth, E., Fobian, Y.M., Gibbs, M.E., Gilles, R.W., Greene, N., Huang, E., Krieger-Burke, T., Loesel, J., Wager, T., Whiteley, L., Zhang, Y., 2008. Physiochemical drug properties associated with in vivo toxicological outcomes. Bioorg. Med. Chem. Lett. 18 (17), 4872–4875.

Johnson, T.W., Dress, K.R., Edwards, M., 2009. Using the Golden Triangle to optimize clearance and oral absorption. Bioorg. Med. Chem. Lett. 19 (19), 5560–5564.

Krishnan, K., Prathiba, K., Jayaprakash, V., Basu, A., Mishra, N., Zhou, B., Hu, S., Yen, Y., 2008. Synthesis and ribonucleotide reductase inhibitory activity of thiosemicarbazones. Bioorg. Med. Chem. Lett. 18 (23), 6248–6250.

Kumar, R., Saneja, A., Panda, A.K., 2021. An annexin V-FITC—propidium iodide-based method for detecting apoptosis in a non-small cell lung cancer cell line. Lung Cancer: Methods Protocols 2279, 213–223.

Lipinski, C.A., Lombardo, F., Dominy, B.W., Feeney, P.J., 2001. Experimental and computational approaches to estimate solubility and permeability in drug discovery and development settings. Adv. Drug Deliv. Rev. 46 (1–3), 3–26.

Madhusudan, S., Ganesan, T.S., 2004. Tyrosine kinase inhibitors in cancer therapy. Clin. Biochem. 37, 618–635.

Mohamed, M.A., Ayyad, R.R., Shawer, T.Z., Abdel-Aziz, A.-A.-M., El-Azab, A.S., 2016. Synthesis and anti-tumor evaluation of trimethoxyanilides based on 4(3H)-quinazolinone scaffolds. Eur. J. Med. Chem. 112, 106–113.

Mosmann, T., 1983. Rapid colorimetric assay for cellular growth and survival: application to proliferation and cytotoxicity assays. J. Immunol. Methods 65 (1–2), 55–63.

Nicholson, R.I., Gee, J.M.W., Harper, M.E., 2001. EGFR and cancer prognosis. Eur. J. Cancer 37, 9–15.

Omar, H.A., Tolba, M.F., Hung, J.-H., Al-Tel, T.H., 2016. OSU-2S/Sorafenib synergistic anti-tumor combination against hepatocellular carcinoma: the role of PKCδ/p53. Front. Pharmacol. 7, 463.

Ormerod, M.G., 2002. Investigating the relationship between the cell cycle and apoptosis using flow cytometry. J. Immunol. Methods 265, 73–80.

Othman, D.I., Hamdi, A., Tawfik, S.S., Elgazar, A.A., Mostafa, A.S., 2023. Identification of new benzimidazole-triazole hybrids as anticancer agents: multi-target recognition, in vitro and in silico studies. J. Enzyme Inhib. Med. Chem. 38 (1), 2166037.

Peterson, Q.P., Hsu, D.C., Goode, D.R., Novotny, C.J., Totten, R.K., Hergenrother, P.J., 2009. Procaspase-3 activation as an anticancer strategy: Structure– activity relationship of procaspase-activating compound 1 (PAC-1) and Its cellular co-localization with caspase-3. J. Med. Chem. 52, 5721–5731.

Regad, T., 2015. Targeting RTK Signaling Pathways in Cancer. Cancers 7 (3), 1758–1784.

Rusnak, D.W., Lackey, K., Affleck, K., Wood, E.R., Alligood, K.J., Rhodes, N., Keith, B.R., Murray, D.M., Knight, W.B., Mullin, R.J., Gilmer, T.M., 2001. The effects of the novel, reversible epidermal growth factor receptor/ErbB-2 tyrosine kinase inhibitor, GW2016, on the growth of human normal and tumor-derived cell lines in vitro and in vivo. Mol. Cancer Ther. 1 (2), 85–94.

Şenkardeş, S., Han, M., Kulabaş, N., Abbak, M., Çevik, Ö., Küçükgüzel, İ., Küçükgüzel, Ş.G., 2020. Synthesis, molecular docking and evaluation of novel sulfonyl hydrazones as anticancer agents and COX-2 inhibitors. Mol. Divers. 24 (3), 673–689.

Son, J., Jang, J., Beyett, T.S., Eum, Y., Haikala, H.M., Verano, A., Lin, M., Hatcher, J.M., Kwiatkowski, N.P., Eser, P.Ö., Poitras, M.J., Wang, S., Xu, M., Gokhale, P.C., Cameron, M.D., Eck, M.J., Gray, N.S., Jänne, P.A., 2022. A Novel HER2-Selective Kinase Inhibitor Is Effective in HER2 Mutant and Amplified Non-Small Cell Lung Cancer. Cancer Res. 82 (8), 1633–1645.

Szakács, G., Paterson, J.K., Ludwig, J.A., Booth-Genthe, C., Gottesman, M.M., 2006. Targeting multidrug resistance in cancer. Nat. Rev. Drug Discov. 5 (3), 219–234.

Takimoto, C.H., Awada, A., 2008. Safety and anti-tumor activity of sorafenib (Nexavar) in combination with other anticancer agents: a review of clinical trials. Cancer Chemother. Pharmacol. 61, 535–548.

Torre, L.A., Bray, F., Siegel, R.L., Ferlay, J., Lortet-Tieulent, J., Jemal, A., 2015. Global cancer statistics, 2012. CA Cancer J. Clin. 65 (2), 87–108.

Uto, Y., Ueno, Y., Kiyotsuka, Y., Miyazawa, Y., Kurata, H., Ogata, T., Yamada, M., Deguchi, T., Konishi, M., Takagi, T., 2010. Synthesis and evaluation of novel stearoyl-CoA desaturase 1 inhibitors: 1'-{6-[5-(pyridin-3-ylmethyl)-1,3,4-oxadiazol-2-yl]pyridazin-3-yl}-3,4-dihydrospiro[chromene-2,4'-piperidine] analogs. Eur. J. Med. Chem. 45 (11), 4788–4796.

Varasi, M., Thaler, F., Abate, A., Bigogno, C., Boggio, R., Carenzi, G., Cataudella, T., Dal Zuffo, M.C., Fulco, M.G.R., 2011. Discovery, synthesis, and pharmacological evaluation of spiropiperidine hydroxamic acid based derivatives as structurally novel histone deacetylase (HDAC) inhibitors. J. Med. Chem. 54 (8), 3051–3064.

Vermes, I., Haanen, C., Steffens-Nakken, H., Reutellingsperger, C., 1995. A novel assay for apoptosis flow cytometric detection of phosphatidylserine expression on early apoptotic cells using fluorescein labelled annexin V. J. Immunol. Methods 184, 39–51.

Vogel, S., Kaufmann, D., Pojarová, M., Müller, C., Pfaller, T., Kühne, S., Bednarski, P.J., von Angerer, E., 2008. Aroyl hydrazones of 2-phenylindole-3-carbaldehydes as novel antimitotic agents. Bioorg. Med. Chem. 16 (12), 6436–6447.

Wang, S., Song, Y., Liu, D., 2017. EAI045: The fourth-generation EGFR inhibitor overcoming T790M and C797S resistance. Cancer Lett. 385, 51–54.

Woodburn, J.R., 1999. The epidermal growth factor receptor and its inhibition in cancer therapy. Pharmacol. Ther. 82 (2–3), 241–250.

Xie, L., Bourne, P.E., 2015. Developing multi-target therapeutics to fine-tune the evolutionary dynamics of the cancer ecosystem. Front. Pharmacol. 6, 209.

Xu, G., Abad, M.C., Connolly, P.J., Neeper, M.P., Struble, G.T., Springer, B.A., Emanuel, S.L., Pandey, N., Gruninger, R.H., Adams, M., Moreno-Mazza, S., Fuentes-Pesquera, A.R., Middleton, S.A., 2008. 4-Amino-6-arylamino-pyrimidine-5-carbaldehyde hydrazones as potent ErbB-2/EGFR dual kinase inhibitors. Bioorg. Med. Chem. Lett. 18 (16), 4615–4619.